Development and Optimization of a Centrifugal Filtration Device for Small Samples

Miguel Maria de Nóbrega Pupo Correia

Thesis to obtain the Master of Science Degree in

Chemical Engineering

Supervisors: Prof./Dr. Vitor Manuel Geraldes Fernandes

Prof./Dr. Miguel Angelo Joaquim Rodrigues

Examination Committee

Chairperson: Prof./Dr. João Carlos Moura Bordado

Members of the Committee: Prof./Dr. Frederico Castelo Alves Ferreira

Prof./Dr. Vitor Manuel Geraldes Fernandes

October, 2019

This page was intentionally left blank

Aknowledgements

This dissertation has been a great challenge, albeit a tremendously fun one, and I'm painfully aware it could never have been possible without the help, support and dedication of a considerable number of people. Thus, I hereby present a list of people whose influence was paramount to this dissertation.

To Professor Vitor Geraldes, for taking me under his wing for these past few months, allowing me to grow and learn. Thank you for all the patience.

To Professor Miguel Rodrigues for all the help provided throughout this project and for allowing me unrestricted access to his lab.

To Professor Marília Mateus, for kindly lending me unlimited access to the centrifuge that was an absolute necessity for this project.

To my parents, Aida and João, and sibling, João Pedro and Rosarinho, for always being there. There aren't many words that can describe how much you've helped, not just now but throughout all my life, but I hope these few can suffice. Truly, thank you!

To my family in Lisbon, who have supported me and who have endured my presence for the past few years in their beautiful city and homes.

To all my friends, for the support and patience, and in particular to Francisco Barata, Gonçalo Ferreira, Bruno Silva, Mariana Ervedosa, Rita Julião, Raquel Nunes and Rita Alves for all the countless hours of brainstorming amidst pointless conversations, without which none of this would be possible.

This page was intentionally left blank

Abstract

Batchwise centrifugal filtration of small samples (<100 mL) for concentration of low molecular weight (MW < 1000 $g.mol^{-1}$) is process that was until recently thought to be unfeasible. Despite recent developments showing it's entirely possible to create a device capable of performing this operation, a commercial option still remains undeveloped.

This dissertation aims primarily at the creation of a commercially viable design for a device capable of performing this operation in an optimized manner. Secondarily, it aims at creating a device capable of performing ultrafiltration operations in a manner that is capable of dealing with protein adsorption and gel-layers formation near the surface of the membrane when non-saline solutions are used.

Such a device was created, with a modular system composed of a fixed base and removable membrane sample chamber was developed. This removable chamber allows for easier prototype preparation and retentate removal, better membrane cleaning and an all-round commercially improved filtration device.

With this device, fair permeate fluxes averaging 3.59 $mL.cm^{-2}.h^{-1}$ were obtained for ultrafiltration tests with a 5wt% solution of PEG35k. The rejection, despite averaging 80.63 % for initial tests where fissures allowed for solute permeation, was increase to 100% when such fissure formation was fixed.

Ultimately, the proposed design is innovative and presents a promising development for the field.

Keywords: Centrifugal nanofiltration; Centrifugal ultrafiltration; Solute concentration; Non-saline protein solutions.

This page was intentionally left blank

Resumo

Filtração centrifuga em *batch* de pequenas amostras (< 100 mL) para concentração de solutos de pequeno peso molecular (MW< 1000 $g.mol^{-1}$) é um processo até agora considerado infazível. Apesar de desenvolvimentos recentes que mostram que é possível criar um dispositivo capaz de fazer esta operação, não existe ainda nenhuma opção comercialmente viável.

Esta dissertação foca-se na criação de um protótipo comercialmente viável capaz de fazer esta operação de forma otimizada. Tornou-se ainda desejável a criação de um dispositivo que, paralelamente à função principal, é capaz de executar operações de ultrafiltração não sujeitas a problemas associados a adsorção e formação de camadas de gel por proteínas na superfície da membrana, usando soluções não-salinas.

Tal dispositivo foi criado, com um sistema modular com uma base fixa e câmara de amostra removível, permitindo fácil mudança de membrana. Este design permite uma mais fácil preparação e limpeza do dispositivo, melhor recuperação de retentado e apresente uma opção comercialmente melhorada em relação aos designs atuais.

Com este dispositivo, bons fluxos de permeado com média de 3.59 $mL.cm^{-2}.h^{-1}$ foram obtidos para testes de ultrafiltração com uma solução de 5wt% de PEG35k. A rejeição, apesar de ter uma média de 80.63 % para testes iniciais onde pequenas fissuras criavam caminhos preferenciais para a solução, aumentou para 100% quando tais fissuras foram eliminadas

Finalmente, o modelo proposto é inovador e demonstra um desenvolvimento interessante neste sector.

Palavras-Chave: Nanofiltração centrifuga; Ultrafiltração centrifuga; Concentração de solutos; Soluções não-salinas de proteínas.

This page was intentionally left blank

Table of contents

List of figures

List of tables

This page was intentionally left blank

List of Abbreviations

CP	Concentration polarisation
MF	Microfiltration
MW	Molecular weight
MWCO	Molecular weight cut-off point
NF	Nanofiltration
PC	Polycarbonate
PEG	Polyethylene glycol
PLA	Polylactic acid
SD	Solution – dilution
SDI	Solution - dilution-imperfection
SF-PF	Surface force - pore flow
PF	Pore flow
RCF	Relative centrifugal force
RO	Reverse Osmosis
UF	Ultrafiltration

List of Symbols[1]

a	Solvent transport parameter for PF model [$m^3.s.kg^{-1}$]
A_e	Effective membrane area [m^2]
A_m	Area of membrane [m^2]
b	Solute transport parameter for PF model [$mol.s.kg^{-1}$]
B	Solute Permeability [$m^{-1}.s^{-1}$]
C	Solute concentration [$mol.m^{-3}$]
CF	Concentration factor [-]
CF_V	Volumetric concentration factor [-]
c_f	Feed-side solute concentration [$mol.m^{-3}$]
c_m	Membrane surface solute concentration [$mol.m^{-3}$]
c_p	Permeate-side solute concentration [$mol.m^{-3}$]
c_r	Retentate-side solute concentration [$mol.m^{-3}$]
dA	Area element of membrane
$d\vec{F}_{centrigugal}$	Centrifugal force exerted by a fluid element [N]
$d\vec{F}_{Coriolis}$	Coriolis force exerted by a fluid element [N]
dm	Mass of a fluid element [kg]
dr	Size of a fluid element [m]
dV	Fluid element [m^3]
D_{vm}	Diffusion coefficient of solvent v into the membrane m [$m.s^{-1}$]
D_{sm}	Diffusion coefficient of solute s into the membrane m [$m.s^{-1}$]
i	Refraction Index [ºbrix]
I	2nd moment of area [m^4]
J_v	Solvent Flux [$m^3.m^{-2}.s^{-1}$]
J_s	Solute Flux [$mol.m^{-2}.s^{-1}$]
J_w	Pure water permeate flux [$m^3.m^{-2}.s^{-1}$]
k_1	Matrix partial permeability for solvent [$m.Pa^{-1}.s^{-1}$]
k_2	Pore partial permeability for solvent [$m.Pa^{-1}.s^{-1}$]
k_3	Matrix partial permeability for solute [$m.s^{-1}$]

[1] The parameters expressed in this table are presented in SI units (including some derived units), but in the main text other common units may be used for convenience.

k_4	Pore partial permeability for solute [m.Pa^{-1}.s^{-1}]
k_c	Effective compression factor
k_v	Feed-membrane partition coefficient of solvent v [-]
k_s	Feed-membrane partition coefficient of solute s [-]
L_P	Hydraulic permeability [m^3.m^{-2}.s^{-1}.Pa^{-1}]
N	Moles of solute [mol]
m	[subscript] Active side of membrane
p	Pressure [Pa]
p	[subscript] Permeate side of membrane
$\overline{p_0}$	Average pressure over the membrane surface on initial moment of filtration [Pa]
P_e	Péclet Number
Q_w	Volumetric pure water flow rate [m^3.s^{-1}]
R	Ideal gas constant [8.314 kg.m^2.K^{-1}.s^{-1}]
$r1$	Radial point of liquid meniscus
$r2$	Radial point of membrane starting point
$r2'$	Radial point of membrane end-point
R_a	Apparent rejection [-]
R_i	Intrinsic rejection [-]
R_m	Resistance of pristine membrane to water permeation [m^{3}m^{-2}]
T	Temperature [K]
t_{run}	Runtime of a trial [s]
V_f	Volume of feed [m^3]
V_p	Volume of permeate [m^3]
V_r	Volume of retentate [m^3]
V_w	Molar volume of solvent w [m^3.mol^{-1}]
$\vec{U}$	Velocity of fluid element [m.s^{-1}]
α	Angle between rotor bucket and axis of rotation [º]
β	Angle between membrane surface and centrifugal force direction [º]
δ_m	Membrane thickness [m]
Δp_{eff}	Effective pressure difference [Pa]
Δp_m	Transmembrane pressure differential [Pa]
$\Delta \pi_m$	Transmembrane osmotic pressure differential [Pa]
μ	Chemical Potential [J.mol^{-1}]
μ_w	Dynamic viscosity of pure water [Pa.s]
π	Osmotic pressure [Pa]
π_f	Feed-side osmotic pressure [Pa]
$\vec{\omega}$	Angular velocity [m.s^{-1}]

Chapter 1: Introduction

Small-volume batchwise centrifugal filtration is a niche field within separation processes that offers a wide variety of applications, from cell filtration, body fluid compounds concentration and protein fractionization/concentration (Pall Life sciences 2003) to a wide variety of applications in pharmaceutical research (Lipnizki 2005; Székely et al. 2013). This process can easily substitute a plethora of other lab-scale separation processes (e.g. alcohol and salt precipitation, electrophoresis, dialysis, column chromatography, etc.) and it does so with versatility, low energy and cost requirements. Despite being able to only process small volumes (< 100 mL), this easily becomes an advantage when expensive solutes are used, or waste reduction is required. While this is an already widely advance field, it is almost exclusively used for ultrafiltration and microfiltration (Baker 2000). However, recent years have shown some development in the field related to batchwise centrifugal nanofiltration (Completo et al. 2017; Hams 2018), which have shown this process is not only feasible, but highly marketable. Completo's design presented an aluminium device that was highly resistant to pressure and allowed for nanofiltration to occur and Hams approached the problem from a disposable point of view, attempting to create a prototype that could be discarded easily and cheaply.

While this process has shown promising, no commercial options exist yet to perform it. The current approaches were held together by either aluminium, which is expensive and not suited for disposable devices, or an excessive amount of glue, which is unsightly, difficult to work with and results in a lesser flux through the membrane. Even with ultrafiltration processes, highly optimized, several problems have appeared with the processing of proteins, specifically the formation of a gel layer or protein adsorption at the membrane surface, which form when no salt is used in the solution and is rather difficult to clean (Porter, 1972).

With all this in mind, this dissertation holds several objectives. First and foremost, it aims to create a functional centrifugal filtration apparatus that can operate at high pressures in order to perform nanofiltration based on a previous design by Hams (2018). Secondly, it aims to optimize said device with focus in minimizing mass transport limitation and functionality. Thirdly, it aims to make this prototype both more user-friendly and commercially viable.

As the project developed, the objective felt a change in direction, with the intention focusing in making a multi-functional device capable of multiple filtration events that range from microfiltration to nanofiltration. This device should be privy to all the limitations of the previous one and be able to function properly at different working conditions, as well as easily contradict protein gel layer formation.

This dissertation, can therefore be outlined into 3 main parts, corresponding to chapters 2 through 5. Chapter 2 examines the theoretical and physical background of pressure-driven membrane processes. It

analyses membrane morphology and performance and how mass-transport occurs within them by detailing several mass-transport models.

Chapter 3 focuses on an historical analysis of batchwise small-volume centrifugal filtration. It analyses the past of this process and the newest developments in the field, and by doing so it describes how and why certain decisions regarding the following chapter were taken.

Chapter 4 and 5 correspond to the bulk of the project, where 5 different models for the proposed prototype were developed sequentially and analysed. These sections also propose several possible advances for future developments of this technique, as well as suggesting a commercially viable solution.

Chapter 2: Pressure-driven membrane processes

Membrane filtration, otherwise known as surface filtration, refers to a separation of substances through a membrane layer (R.W. Baker 2000; Sahai 2000; Scott 1995a).This layer allows for the permeation of certain substances while retaining others above the membrane surface. This way, it's possible to separate substance based on size exclusion through the membrane, in order to concentrate the retentate (above the membrane) or to filter it away from the permeate (bellow the membrane).

All membrane filtration needs to be driven by a transmembrane difference in chemical potential (μ) known as a driving force. This driving force can be induced by several parameters, from concentration differences to temperature gradients, but this work focusses on pressure-driven processes. As the name indicates, the driving force behind them is a pressure difference between the feed and the permeate sides of the membrane.

Due to the ample nature of this process, it is often separated into four main categories: Microfiltration (MF), Ultrafiltration (UF), Nanofiltration (NF) and Reverse Osmosis (RO) (Figure 1). Despite being similar, due to the physical processes surrounding them being fundamentally the same, this differentiation arises from a difference in solute weight for which each process is used, as well as the intrinsic characteristics of the processes that allow for this weight difference to be felt (Baker 2000).

Microfiltration used to separate small particles (0.1 - 10 μm) from a suspension. Due to working mainly under the size exclusion principle (SEP), with large pores, they can be operated at low pressures (Δp_m < 2 bar).

Ultrafiltration processes, used for colloids and macro-molecules with a size larger than 2000 $g.mol^{-1}$, are also operated under relative low pressures, between 1 and 10 bar and also work through SEP similarly to MF.

Nanofiltration offers a reliable separation method for small molecules with 200 $g.mol^{-1}$ < MW < 1000 $g.mol^{-1}$ and for bivalent ions through the action of electrostatic forces. Due to the smaller pore diameter, it requires Δp_m between 10 and 30 bar for reliable use.

Reverse Osmosis is practically equal to NF, but it has higher rejection rates towards monovalent ions and, depending on the osmotic pressure it's put under, can operate up to 100 bar.

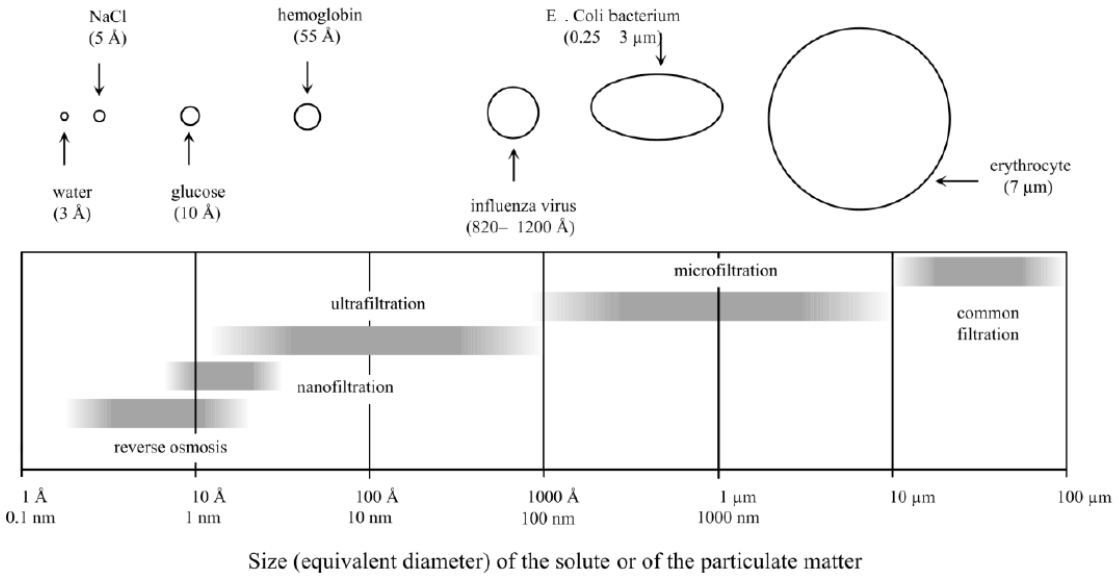

Figure 1 - Size comparison of typical particles and the correspondent pressure driven membrane processes needed to filter them out of a solution (Completo 2018).

This chapter will be exploring the nature of the membrane layer, the physical principles surrounding these processes and the models needed to understand them, and analysing a few challenges surrounding the subject.

2.1 Membrane characterization

2.1.1 Polymeric membranes:

Membranes can be either polymeric, ceramic or metallic in nature. Ceramic and metallic membranes are often regarded as being more durable, more stable and less prone to fouling, amongst other advantages. However, they tend to be heavy and brittle as well as more expensive than polymeric membranes. For these reasons, polymeric membranes are often the preferred kind in pressure driven membrane processes (Dickhout et al. 2017; Scott 1995b).

Morphologically, these membranes can be symmetric – dense and porous – or asymmetric – integrally skinned and thin-film composite (Figure 2) (Baker 2004).

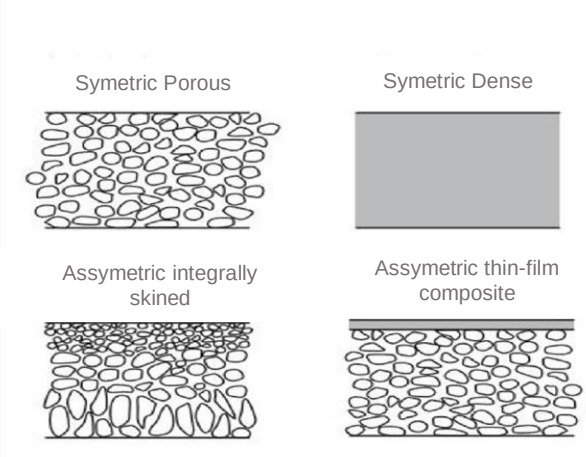

Figure 2 - Sketch of the morphological structure of different membranes (Adapted from Baker 2004)

Dense membranes consist of a polymeric matrix with no pores and the flow through the membrane happens solely through diffusion. Since the filtration isn't based on the size exclusion principle, these membranes are the best for separating similarly sized solutes, mostly in RO. Porous membranes, on the other hand, allow small solutes to permeate through the pores while rejecting larger particles. These are mostly used for MF and UF.

Integrally skinned and thin-film composite membranes both work under the principle that the membrane thickness is inversely proportional to the transport rate and approach it similarly by lodging a thin membrane (0.1 to 1.0 μm) above a less dense support, thus maintaining physical integrity without relinquishing high flow rates. Integrally skinned membranes have a dense, yet still porous upper layer, most appropriate for MF and UF processes, while thin-film composite membranes have a denser, non-porous film, best suited for NF and RO. Most industrial processes nowadays use asymmetric membranes due to higher flow rates being more economically viable.

2.1.2 Performance:

In order to properly evaluate pressure-driven membrane processes, two parameters need to be studied regarding the performance of any given membrane: Hydraulic permeability and solute permeability.

The former, hydraulic permeability (L_P), can be seen as an innate property of a new and fresh membrane (Porter 1990). It refers to the flux of pure water in said membrane per unit of transmembrane pressure and is therefore highly related to the pure water permeate flux, J_w, given by:

$$J_w = \frac{Q_w}{A_m} \qquad (2\text{-}1)$$

where Q_w is the volumetric water flow and A_m is the membrane area. L_p can then be calculated by factoring in the transmembrane pressure.

$$L_p = \frac{J_w}{\Delta p_m} \tag{2-2}$$

Because the pressure gradient is the driving force that induces water movement from one side of the membrane to the other, the water flux is expected to increase with added transmembrane pressure. As such, L_p gives us an unbiased look at the flow through any particular membrane, regardless of the pressure used.

Using L_p it's also possible to calculate the membrane's resistance to water permeation, R_m (Carman 1997):

$$R_m = \frac{1}{\mu_w . L_p} \tag{2-3}$$

where μ_w is the dynamic viscosity of pure water. As the resistance increases with fouling, we can expect L_p to decrease with use. This explains why L_p of a membrane is always calculated for pristine membranes (Rudie, Torgrimson, and Spatz 1985).

As for solute permeability, it allows us a glimpse into the membrane's efficiency and selectivity. A good measure of this parameter can be obtained by measuring rejection coefficients.

Apparent rejection (R_a), otherwise known as observable rejection, is defined as the percentage of solute retained above the membrane:

$$R_a = \frac{c_f - c_p}{c_f} = 1 - \frac{c_p}{c_f} \tag{2-4}$$

where c_f and c_p are the solute concentration of feed stream and permeate stream. Any given membrane working under the size exclusion principle can be characterized by a molecular weight cut-off point (MWCO), which corresponds to the molecular weight for which the rejection will be 90%.

Since R_a depends on operating parameters, intrinsic rejection (R_i) is also sometimes used, which uses solute concentration at the membrane surface (c_m) rather than feed concentration.

$$R_i = \frac{c_m - c_p}{c_m} = 1 - \frac{c_p}{c_m} \quad (2\text{-}5)$$

However, R_i is far more useful when dealing with cross flow filtration, where c_m can easily be determined through the use of film-theory (Murthy and Gupta 1997). In dead-end filtration, where membrane concentration changes throughout the process, this parameter becomes far less useful for the present work.

2.2 Mass transport through the membrane

As seen in section 2.1.2, dead-end filtration requires a comprehensive knowledge of mass transport phenomena through the membrane layer. A multitude of models have been created to properly describe the inner workings of membrane processes. This section aims to give an overview of some of these models which prove to be most appropriate for the project at hand.

2.2.1 Osmotic pressure model:

The simplest model to deal with membrane filtration, the osmotic pressure model as laid out by Kedem and Katchalsky (1961), relates the solvent flux through the membrane and the effective pressure difference (Δp_{eff})

$$J_v = L_P . \Delta p_{eff} \quad (2\text{-}6)$$

Δp_{eff} is a pressure-driven force between the active side (inhere after symbolised as m) and permeate side (inhere after symbolised as p) and can be calculated as $\Delta p_{eff} = p_{eff,m} - p_{eff,p}$. Δp_{eff} considers both applied pressure (p) and osmotic pressure (π), such that

$$\begin{aligned} p_{eff,m} &= p_m - \pi_m \\ p_{eff,p} &= p_p - \pi_p \end{aligned} \quad (2\text{-}7)$$

Considering $\Delta p_m = p_m - p_p$ and $\Delta \pi_m = \pi_m - \pi_p$, equation (2-6) can be re-written as

$$J_v = L_P.(\Delta p_m - \Delta\pi_m) \quad (2\text{-}8)$$

The osmotic pressure can be calculated using Lewis's equation (Lewis 1908)

$$\pi = \frac{R.T}{V_w}.\left(\frac{N}{1-N}\right) \quad (2\text{-}9)$$

2.2.2 Solution-Diffusion model:

For membranes with dense active layers, as is the case with most NF and RO membranes, this model, which considers a symmetric dense membrane where each solvent and solute dissolve into the membrane according to their partition coefficient and diffuses according to their own concentration and diffusion gradients is more applicable. This model also considers the pressure inside the membrane to be equal to the feed-side pressure (Wijmans and Baker 1995).

By relating the hydraulic permeability of the membrane with some physio-chemical properties of both the membrane and the solvent (namely diffusion coefficient of the solvent and of the solute in the membrane D_{vm} and D_{sm}, feed-membrane partition coefficient of the solvent k_v and solute k_s, solvent molar volume V_v, solute permeability B and the membrane's thickness δ_m), the fluxes can be calculated as

$$J_v = L_P.(\Delta p_m - \Delta\pi_m) = \frac{k_v.D_{vm}.V_v}{\delta_m.R.T}.(\Delta p_m - \Delta\pi_m) \quad (2\text{-}10)$$

$$J_s = J_v.C_P = B.(c_m - c_p) = \frac{k_s.D_{sm}}{\delta_m}.(c_m - c_p) \quad (2\text{-}11)$$

where R is the ideal gas constant and T the temperature. Considering equations 2-11 and 2-5, one can calculate the intrinsic rejection as:

$$R_i = \frac{J_v}{J_v + B} \quad (2\text{-}12)$$

By observing the equation, it becomes obvious that rejection increases with a permeate flux increase. Furthermore, since permeate flux is pressure dependent and solute flux isn't, the rejection will increase with transmembrane pressure. A further consequence of this model is that as the difference between Δp_m and $\Delta\pi_m$ decreases, the rejection highly decreases, regardless of the magnitude of CP.

2.2.3 Solution-Diffusion-Imperfection model:

The SDI model, proposed by Sherwood et al. (1965), considers that although most of the membrane is dense and homogeneous, some pores and other imperfections exist on its surface. Both solvent and solute can permeate through these imperfections with no change in solute concentration, as seen in Figure 3, and therefore equations 2-10 and 2-11 need to be corrected to account for this extra flow

$$J_v = k_1.(\Delta p_m - \Delta\pi_m) + k_2.\Delta p_m \quad (2\text{-}13)$$

$$J_s = k_3.(C_m - C_p) + k_4.\Delta p_m.C_m \quad (2\text{-}14)$$

where k_1 and k_3 are membrane matrix partial permeabilities for solvent and solute respectively, and k_2 and k_4 membrane pores partial permeabilities for solvent and solute respectively

Since we can consider the $R_i \approx 0$ on the pores, where $C_m \approx C_p$, the overall rejection of the membrane is also lower than the one calculated through the Solution-Diffusion model. As could be expected, the more imperfections within the membrane, the less it can reject any given solute.

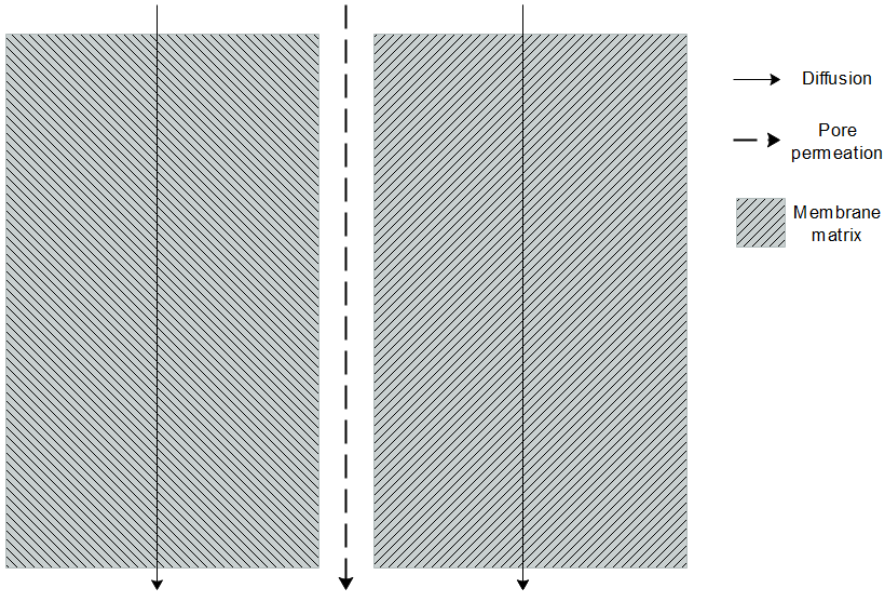

Figure 3 - Illustration of solute movement according to the standard SDI model.

2.2.4 Revised Solution-Diffusion-Imperfection model:

As a response to the standard SDI model, Yaroshchuk (1995) noted that due to interactions between the matrix and the pores, even under perfect conditions where the selectivity in the imperfections is non-existent ($C_m = C_p$), the solute is bound to diffuse through imperfections towards the matrix (Figure 4).

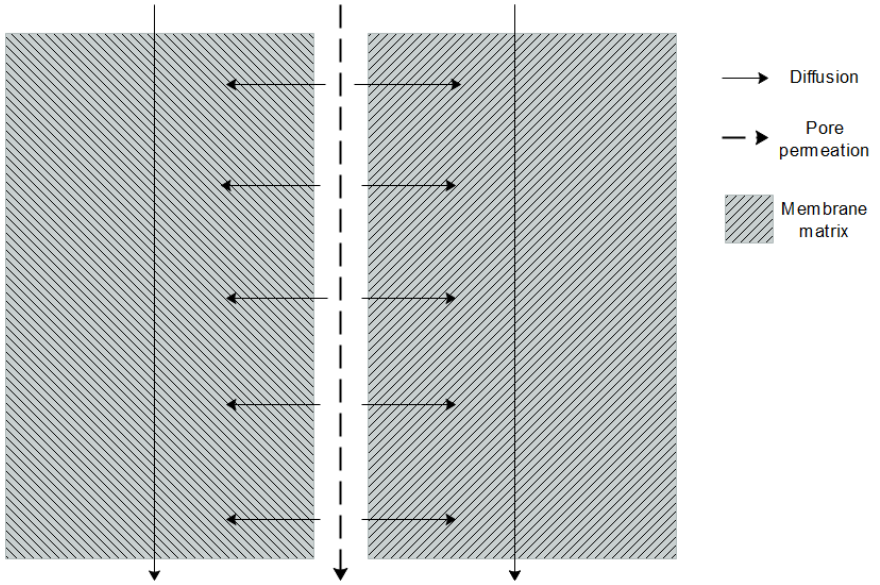

Figure 4 - Illustration of solute movement according to the modified SDI model.

Due to this lateral diffusion, a slight adjustment to the solute flux calculations is required, such that:

$$J_s = k_3.(C_m - C_p) + k_4.\Delta p_m.\frac{C_m - C_p.e^{-Pe}}{1 - e^{-Pe}} \qquad (2\text{-}15)$$

P_e represents the Péclet number, a function of the Reynolds and Schmidt numbers of the flow within the pores that describes the quotients between advective and diffusive forces

As $Pe \rightarrow \infty$ this model will tend to the standard DSI model. This will occur when the pore radius is larger, thus decreasing the diffusion area. Equally, when the membrane is less dense, thus increasing the diffusional permeability parameter k_3, the effects of the imperfections will be less felt, and the model will become similar to the standard DSI model.

Therefore, this model is most needed when working with denser membranes with small and numerous imperfections.

2.2.5 Electrokinetic models:

SD models are severely limited when they encounter multiple forces interacting. In membrane processes, this fact becomes blatantly obvious when dealing with charged solutes, like salts, that interact with charged polymeric NF membranes.

The existence of electrostatic forces between the ions and the membrane, in addition to the pressure difference that governs the filtration process, calls for complex models that couple both forces in order to determine the flux of each ion involved (Tsuru et al. 1994).

2.2.6 Pore Flow models:

Unlike the previously explored SD models, pore flow models assume constant solute concentration across the membrane. Especially useful for MF and UF processes, they model less dense membranes as an impermeable matrix where no diffusion occurs and semi-permeable pores that exclusively filter according to the size exclusion principle.

As such, these models rely on a pressure gradient to serve as a driving force. The simplest model, conveniently known as the pore flow model (Okada and Matsuura 1991), relies on Darcy's law to calculate the fluxes as:

$$J_v = \frac{a}{\delta_m} . \left(p_m - p_p\right) \tag{2-16}$$

$$J_s = \frac{b}{\delta_m} . \left({p_m}^2 - {p_p}^2\right) \tag{2-17}$$

where a and b represent phase transport parameters for the solvent and the solute respectively.

Several other pore flow models have been suggested, such as the Banerjee-De model (Banerjee and De 2010), the surface force-pore flow model (SF-PF) (Matsuura and Sourirajan 1981) and even a modified SF-PF model (Mehdizadeh and Dickson 1989), which dive deeper into the pore flow by analysing friction forces, membrane-solute interactions or even considering PF-SD hybridization methods, but for the standard porous membranes the PF model achieves satisfactory results without having to rely on complex numerical algorithms or simulations (Wang et al. 2014).

2.2.7 Mass-transfer models overview:

Engaging as these models may be from an intellectual point of view, that hardly speaks to their validity in real world applications and more importantly, their validity within this work. Pore flow models are reliable for porous membranes but require transport parameter lab tests and complex computations if one wants a reliable model. Kinetic models present an optimal approach for charged solutes in NF membranes, which were not used in any tests throughout this dissertation. The SD models (SD, DSI and revised SDI models) present several approaches for modelling NF and RO membranes that have proved quite accurate in a multitude of scenarios. However, despite having used NF membranes, these models again require lab testing and/or complex calculations, which present out of the scope of the present work. As such, the model used for this project was the osmotic pressure model. Despite being the simplest of the above mentioned models, it considers the highest limitation to transport, the osmotic pressure, which for the short pulsed trials further detailed in chapter 4 is more than necessary to properly model the system.

That being said, if and when a commercial application of the work developed in this dissertation is embraced, a proper research on the best membranes to be used should be performed and a more optimal model should be applied.

2.3 Mass transport limitations

Under ideal conditions, the membrane layer would be the only resistance the fluid finds during the filtration process. However, in real processes, the mass transport becomes limited by several phenomena that need to be mitigated in order to ensure the optimization of any given process. Four such phenomena, holding particular interest for the process at hand, are further detailed in this subsection.

2.3.1 Fouling

Simply put, continuous or repetitive use of a membrane can lead to a deposit of unwanted matter to build up over time on the membrane surface and/or within the pores. These build up processes are collectively referred to as fouling (Ao et al. 2016). By creating resistance to mass transport, fouling will decrease the solvent flux and, as observed by equation 2-12, decrease the rejection of the process.

Fouling can be caused by a plethora of phenomena. Biofouling can be cause by microbial growth, incrustations can appear due to compounds precipitating and suspended particles can form a cake above the membrane surface, for instance. Most membrane filtration processes will eventually undergo some type of fouling.

To avoid this flux decrease the membrane can be periodically cleaned to remove surface fouling, or substituted entirely if the fouling is difficult to remove without damaging the membrane. Cleaning methods

include chemical cleaning (e.g. solvent soaking) and mechanical cleaning (e.g. backwashing[2]) (Abdelrasoul, Doan, and Lohi 2013). Fouling can also be mitigated through pre-treatment of the filtration feed. The nature of said treatment varies with the process, and often includes coagulation and sedimentation/filtration of larger particles.

2.3.2 Gel Polarization

Though technically a type of fouling, several authors have felt it necessary to point out this phenomenon as being of particular interest (Ahmad 2012; Kozinski and Lightfoot 1972; Porter 1972). Most prominent in UF processes involving proteins and polysaccharides, where gelling can occur through rheological changes (Barr and White 2006) as well precipitation due to high applied pressure increasing solute concentration above the membrane, this gel layer can not only drastically reduce permeate flux, but be incredibly hard to remove from the membrane, irreversibly damaging it and leading to a reduced retentate concentration, which can be less than ideal.

The addition of anti-gelling agents, such as NaCl, can be a possible solution to this problem (Susanto et al. 2008). However, for certain processes this can be undesirable, so other methods of stopping this gel formation must be employed.

One such method is centrifugal filtration, which drags away the protein particles and avoids build--up around the membrane surface and pores. Currently existent designs are still unable to do this, as they tend to be symmetrical rather than directional, meaning particles dragged from one side tend to adsorb to another.

[2] Process through which solvent flow is reversed in order to drag solids away from membrane surface.

2.3.4 Membrane Compaction

Compaction refers to the irreversible compression of a membrane under excessive pressure (Volkov 2014). When this happens, the decrease of initial transport parameters can be felt, and the relationship between flow through the membrane and the pressure will stop being linear and start curving downwards, as illustrated in Figure 5.

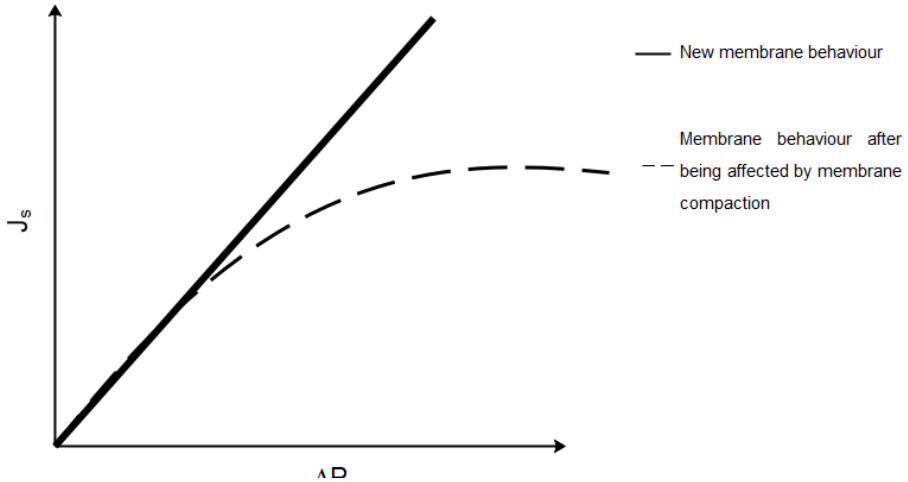

Figure 5 - Effects of membrane compaction on the solvent flux.

This effect cannot be mitigated once brought out. Therefore, one must take extra care not to exceed the pressure of membrane compaction of any given membrane. This pressure value varies from membrane to membrane, depending on porosity and thickness, but a good rule of thumb is to not exceed the maximum working pressure suggested by the manufacturer.

2.3.3 Concentration Polarization

When pressure is exerted over a membrane during filtration, there is a tendency for particles to be pushed against the membrane surface and accumulate around it, limiting mass transfer. In porous membranes, this leads to pores being plugged, while compact ones felt diffusion resistance (Figure 6). This phenomenon is more widely known as Concentration Polarization (CP) (Luis 2018).

This has two main consequences. As the osmotic pressure increase near the membrane (since the concentration increases) so does $\Delta\pi_m$, and with it the driving force for the permeating particles will decrease,

while the driving force for the rejected solutes will increase. This will ensure a drop in both permeate flux and rejection (Sherwood et al. 1965).

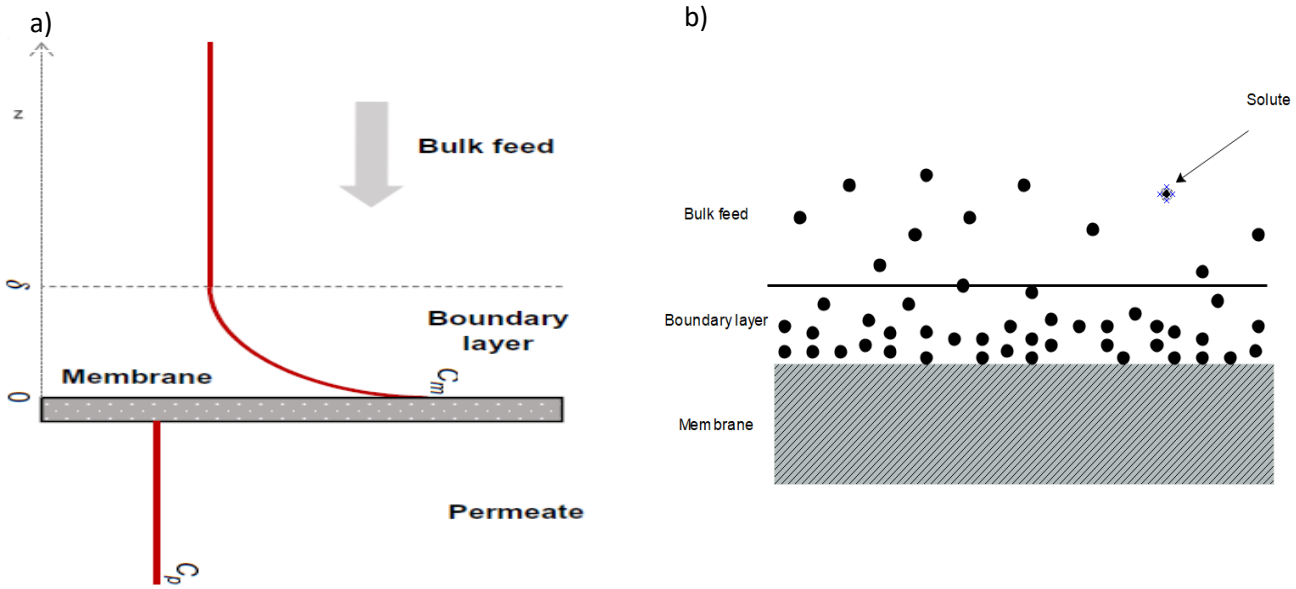

Figure 6 - Concentration polarization adjacent to a membrane during dead-end filtration: a) visualization of concentration gradient (adapted from Luis 2018); b) visualization of solute movement.

The key to avoiding this build-up of CP is to promote mixing between the feed and the boundary layer, thus allowing the particles to dislodge away from the membrane and flow back into the feed. This becomes especially important in dead-end filtration, where the CP will eventually lead to the absence of flow entirely. This can be done by several methods, such as static mixers, feed pacers, pulsating flow or irregular feed path (Hilal et al. 2005), all useful for different filtration conditions and purposes.

Centrifugal filtration is a fantastic method of mitigating CP. As will be seen in section 2.4, this method allows for a “self -cleaning” effect over the membrane surface, by which the solute particles are dragged away from the surface by the centrifugal force acting on them. This effectively creates mixing without the need to use external pumping, baffles or mixers, drastically reducing the volume needed for effective filtration.

2.4 Centrifugal filtration

2.4.1 Basic principles

Centrifugal filtration, dissected to its simplest terms, is the rotation of a filtration device around an axis. This rotation generates the main driving force of the process, a transmembrane pressure difference.

Although both sides of the membrane are exposed to atmospheric pressure, the fluid above the membrane, while it is in rotation, exerts enough hydrostatic pressure above the membrane to allow permeation (Svarovsky 2001). This pressure can be calculated thusly:

Consider an incompressible fluid element, dV, of mass dm. At a position r away from the rotation axis (rotating with constant angular velocity ω), this element will exert a pressure dP above the membrane.

$$dp = \rho.\omega^2.r.dr \tag{2-18}$$

If we consider the limits of the fluid element as r1 and r2, then the pressure difference generated is calculated as:

$$\Delta p = \int_{r_1}^{r_2} dp = \int_{r_1}^{r_2} \rho.\omega^2.r.dr = \frac{1}{2}.\ \rho.\omega^2.(r_2^2 - r_1^2) \tag{2-19}$$

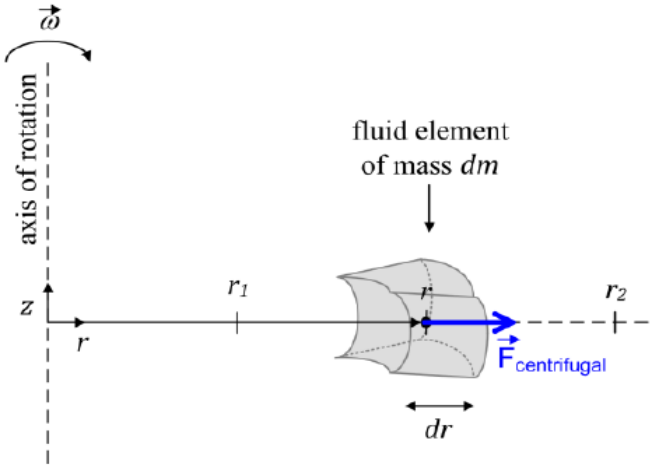

Figure 7 - Lateral view of a fluid element rotating around an axis (Completo 2018)

Since these devices tend to have an angle, β, the pressure measurement varies from one edge of the membrane to the other. In addition, the pressure drops during filtration due to a reduced fluid volume. As such, all processes for these devices are characterized by the average pressure over the membrane on the initial point of filtration, $\overline{p_0}$, which can be calculated by integrating equation 2-18 over the membrane area.

$$\overline{p_0} = \frac{\iint_{A_m} \Delta p.dA}{\iint_{A_m} dA} = \frac{\int_{r2}^{r2'} \int_{-\sqrt{b^2.(1-(x-c)^2/a^2)}}^{\sqrt{b^2.(1-(x-c)^2/a^2)}} \frac{1}{2}.\rho.\omega^2.\left(\left(\sqrt{x^2+y^2}\right)^2 - r1^2\right).dy.dx}{\int_{r2}^{r2'} \int_{-\sqrt{b^2.(1-(x-c)^2/a^2)}}^{\sqrt{b^2.(1-(x-c)^2/a^2)}} .dy.dx} \tag{2-20}$$

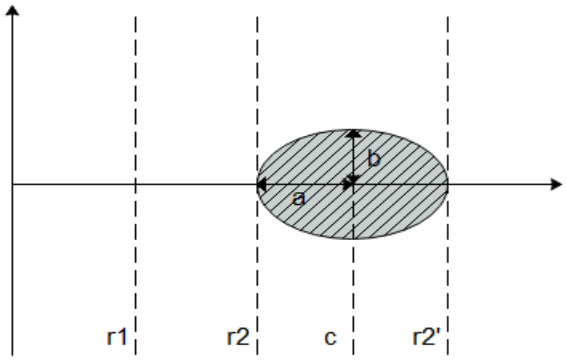

Figure 8 - Sketch of positions of interest on the centrifugal device. R1 is the liquid meniscus, r2 and r2' are the edges of the membrane and c is its centre.

Although a pressure difference would be enough to allow filtration, if this compression force was the only force present the particles would be squished heavily against the membrane and create the before mentioned mass transport limitations. So, where does this so called “Self-cleaning mechanism” come from? The answer lies in the existence of centrifugal and Coriolis forces (Figure 9), as calculated by:

$$d\vec{F}_{centrigugal} = -dm \times \vec{\omega} \times (\vec{\omega} \times \vec{r}) \quad (2\text{-}21)$$

$$d\vec{F}_{Coriolis} = -2.dm \times \vec{\omega} \times \vec{U} \quad (2\text{-}22)$$

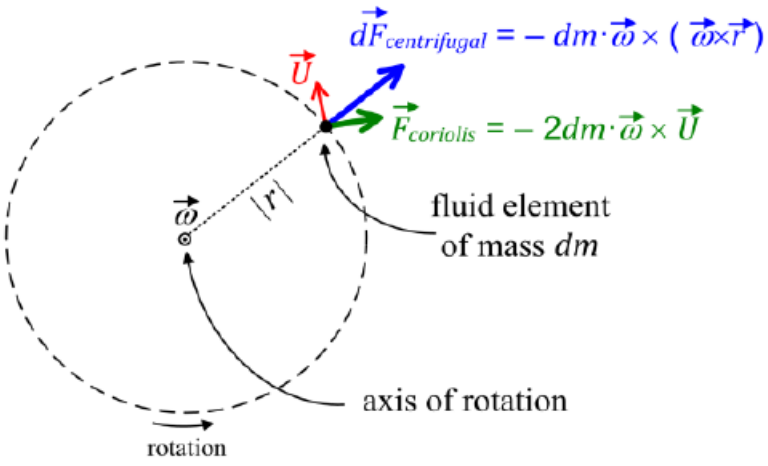

Figure 9- Overtop view of a fluid element rotating around an axis (Completo 2018)

Centrifugal Force refers to the force dragging the fluid element away from the axis of rotation, and the Coriolis force refers to the fictional force that describes the actual movement of the fluid element. Since these forces are linearly dependent to the mass of the element, heavier particles will succumb to a larger effect, meaning if the membrane is angled away from the angle of rotation, the solutes will tend to be swept away from the membrane surface, allaying CP and fouling. Since these forces are much larger than the force of gravity, this becomes negligible and the particles are mainly dragged by the rotational movement. Calculating how negligible gravity is when compared to the centrifugal force can be done by using the rotational centrifugal force parameter (RCF),

$$RCF = \frac{centrifugal\ force}{gravitational\ force} = \frac{r.\omega^2}{g} = \frac{r.(2\pi.RPM)^2}{60.g} \quad (2\text{-}23)$$

2.4.2 Sample concentration

There are two main things that can be recovered from a filtration process. The first is the permeate, clear of solute. The second is the retentate, rich in solute. The one of most interest for the device being created for this dissertation is the later.

Since concentrating a retentate is the main purpose, a parameter was used to determine how rich in solute it can become, the concentration factor CF, defined as the ration between the concentration of the permeate and the concentration of the feed

$$CF = \frac{c_r}{c_f} \quad (2\text{-}24)$$

and the volumetric concentration factor.

$$CF_V = \frac{V_r}{V_f} \quad (2\text{-}25)$$

For the cases where $R_a = 100\%$, the concentration factors will have the same value.

Chapter 3: Previous advancements in small-volume centrifugal filtration

Centrifugal filtration for concentration of small samples has found ample use in several fields, including biological and pharmaceutical research. For this reason, the concept has had several advances in the last few years. This chapter will be exploring how it came to be and how it developed throughout the years. By understanding the past, one hopes to improve the future of this ever-growing field.

3.1 The beginnings of lab-scale batch centrifugal filtration

In 1970, a man by the name of Peter Rigolupos published a patent entitled “Self-cleaning Ultrafilter” (Rigolupos 1970; Figure 10), which he described thusly:

«Novel self-cleaning ultrafiltration apparatus comprising an anisotropic membrane mounted on a foraminous support that, when placed in a centrifuge device, a major component of the centrifugal force tends to wipe the membrane clean during the filtration action» – Rigolupos, 1970

The described object was an early device that made use of the principles behind what later came to be known as centrifugal UF, with aim to make a self-cleaning membrane. By creating a support full of small holes (“foraminous”), a membrane was allowed to rest at an α (centrifuge angle) and β (membrane angle) no larger than 15.0º and 22.5º respectively against a permeable surface and rotated around an axis, pushing the macromolecules away from the membrane.

The main aim of this device was to improve filtration of protein solutions to achieve a better permeate cleanliness for a small amount of solution. This was of particular importance when dealing with unstable and active biological material, where waste could not just be costly, but also dangerous. So far, the few methods to perform this operation included chemical precipitation and evaporation, and any devices that made use of asymmetric UF membranes required a much larger size to mount a stirring apparatus to avoid CP, but all these required extreme care not to damage the solute and had large associated costs. Although biological processes were the main focus, Rigolupos himself stated that he saw use in other areas related to macromolecule and colloid filtration.

Having obtained fantastic results, with rejections of 100%, this device still possessed a massive flaw: Filtration to dryness was unavoidable for long enough tests, which due to its small volume capacity (around 3 mL) was bound to happen rather quickly.

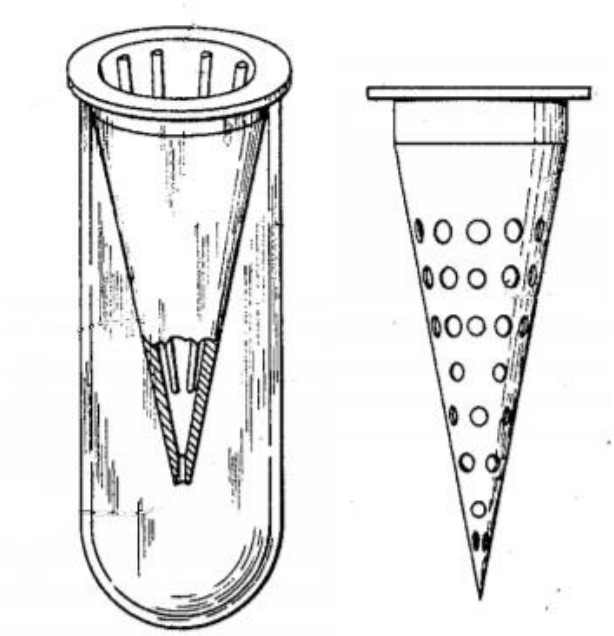

Figure 10 - Sketches of Rigolupos' device (Rigolupos 1970)

Despite its flaws, Rigolupos' device came to revolutionize how separation processes were performed at a lab scale and is the basis for all other devices invented in the past 60 years. Without it, it's a certainty that not only would the field of small-scale batch centrifugal filtration be severely lacking (if at all existent), but plenty of other fields would have been severely hindered as a result.

3.2 Advances in large-solute filtration

Countless developments were made in the field of batchwise centrifugal UF over the past half a century. To simplify the analysis of these developments and to keep to the point of this chapter, this section focusses on just a few devices, and divides the main advances on centrifugal filtration batch devices into four major areas: prevention of filtration to dryness; Separation of concentrate from the membrane; Membrane placement; And membrane area maximization. It goes on to give a few examples of inventors who pursued these advances

Filtration to dryness occurs whenever the whole solvent passes through a membrane resulting in a dry sediment on the membrane surface, or even in its deposition in the internal structure of the membrane. Despite being possible to re-dissolve the sediments, filtration to dryness usually leads to low recovery of the substances that one desires to concentrate. To this effect, one major advance was shown to be a solution to this problem. Bowers and Rigolupos (1986) proposed an alteration to Rigolupos' initial design (Rigolupos 1970) wherein a small section on the lower part of the conical membrane support was left impermeable, allowing the liquid meniscus to drop beneath the membrane at a certain point, stopping the filtration (Figure 11 -a). This way, filtration to dryness was easily avoided.

Bower and Rigolupos' design still allowed, however, contact between the membrane surface and the concentrated retentate. The separation of this retentate from the membrane was therefore still a necessity, as it alowed for losses of solute through adsorption, which not only made the final retentate less concentrated, but also fouled the device heavily. Several authors suggested solutions to this problem, mostly in regards to new and improved concentrate chambers. Vassarotti (1997) (Figure 11- b) and Bonhomme et al. (2014) (Figure 11 -c) found that by placing this retentate chamber on the outermost radial position with respect to the membrane, the retentate would be pushed away from the membrane, mitigating this effect.

Regarding membrane placement, this factor plays a massive role in the performance of any given device. The best results seem to have been found when the membrane is parallel or angular to the axis of rotation (Vassarotti 1997; Bonhomme et al. 2014)

Lastly, membrane area maximization has been adopted by several authors as a method of maximizing flow through the membrane, hence minimizing user time wasted. Conical and cylindrical membrane segments are often used as they have a higher area-volume ratio on the sample chamber (Bowers, Yankoupoulos, and Towle 2001) (Figure 11 - d), but even some designs that use rectangular membranes tend to maximize area by using two rectangular segments facing each other, effectively doubling the membrane area, even if one side is far less effective than the other (Bonhomme et al. 2014).

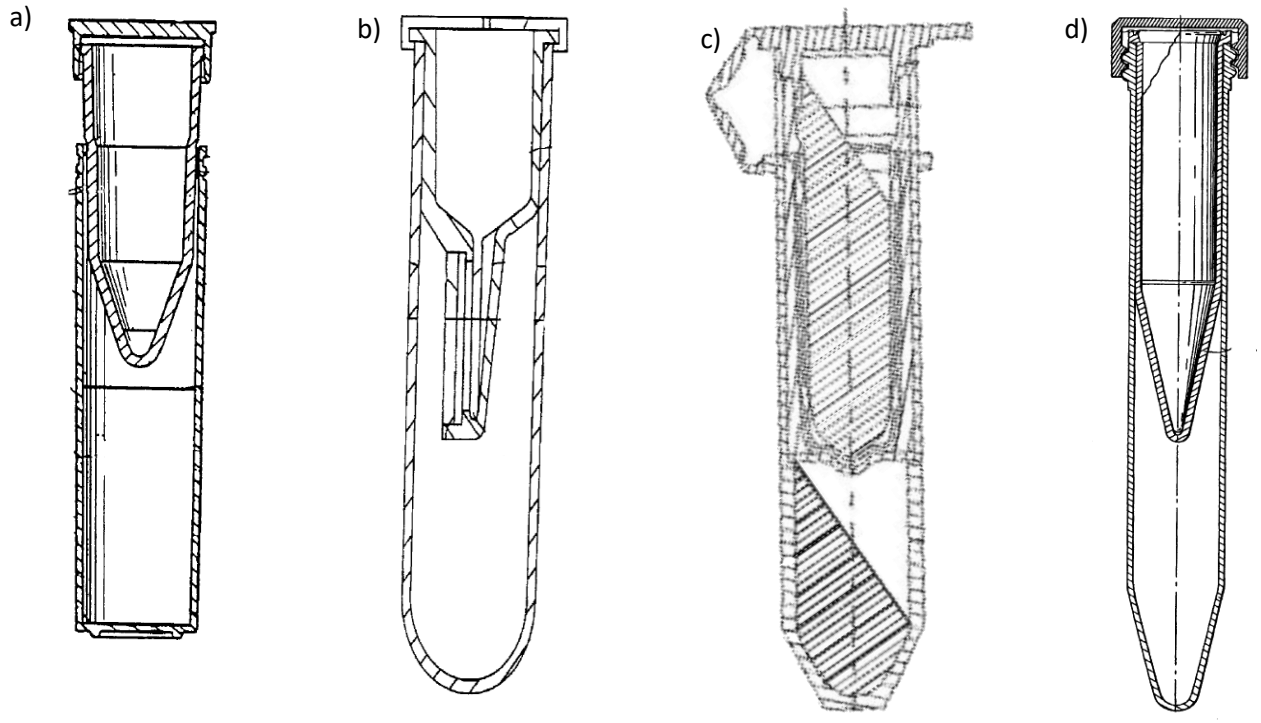

Figure 11 - A few centrifugal UF devices developed throughout the years to address different issues. a) Bowers and Rigolupos (1986); b) Vasseroti (1997); c) Bonhomme et al (2014); d) Bowers, Yankoupoulos, and Towle (2001).

3.3 Stepping into Nanofiltration

While several options are available for centrifugal MF and UF, for reasons already addressed, no commercial NF devices for processing small samples are yet available. The developments in the field are still fairly recent, but already show a vast amount of promise.

An early proof of concept was developed by Completo et al. (2017), where an aluminium shell was fitted with a membrane support and collection chamber and a 3D printed polylactic acid block. This block extended the sample chamber and minimized its volume, in order to maintain points r1 and r2 of the device as far apart as possible for as long as possible, which had the effect of maintaining high transmembrane pressure throughout the process (Figure 12).

By keeping the membrane flat against a nearly solid support (apart from one permeation point), creating a back flow channel for increased mixing of concentrate and feed sample, and by maintaining a large pressure throughout the process, Completo's prototype served as a demonstration that it was not only possible to process small samples through centrifugal NF, but that one such device could achieve CF as high as 20 while maintaining desirable rejection factors.

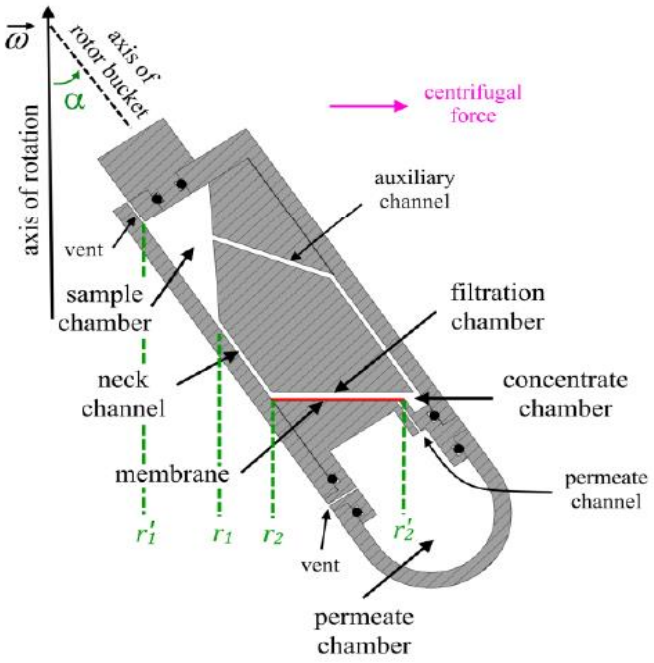

Figure 12 - Detailled drawing of Completo's design for an early concept of a centrifugal NF design (Completo et al 2017)

The creation of a commercially viable centrifugal NF device was then attempted by Hams 2018, who developed a prototype with a polycarbonate shell and 3D printed polylactic acid membrane support and inner block. The device was conceptually similar to Completo's approach but differed in a few key aspects, as depicted in Figure 13.

Firstly, the device was designed to be disposable and was made in plastic, and as such the membrane support needed to be glued or connected to the shell somehow. Hams selected a 2-part epoxy for this purpose. Secondly, the concentrate chamber was eliminated from the membrane support design and was instead added to the inner block (Figure 13). This chamber is fictitious and exist as the entire volume bellow the permeation point in the support.

This device showed promising, being able to properly process the sample. However, due to limitations of the gluing and design of the device, it was only able to achieve relatively small permeate flux rates (10^{-1} mL.cm^{-2}.h^{-1}), albeit with a good rejection factor, and consequentially only managed a maximum CF of around 5.

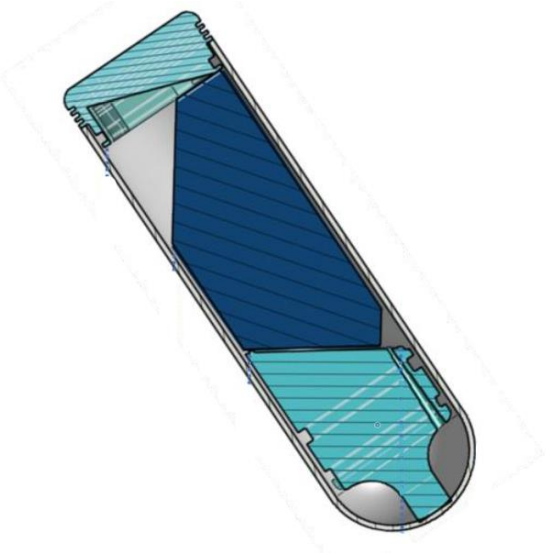

Figure 13 - Diagram of Ham's design for a centrifugal nanofiltration device for concentration of small samples (Hams, 2018)

These two devices served as great inspiration for the designs established hereon in this dissertation and laid the foundations for what became the final device presented in this work. Without their approaches and efforts, it would be nigh impossible to even start this project, let alone finish it. For this reason, these two projects are sited a reasonable number of times throughout this dissertation, especially when justifying certain approaches

This page was intentionally left blank

Chapter 4: Prototype Development

This chapter will be exploring the development process of the prototype proposed by this thesis, by detailing the methods used to improve on the previous models. The starting point for this project was the model provided by Hams, 2018 as described at the end of chapter 3.

4.1 Methods

4.1.1 Device manufacturing through 3D printing

Apart from the device's outer shell, all the parts required were manufactured in Smartfil Polylactic acid filament (Smartfill 2019; Table 1) using a Ultimaker 2+ 3d printer. The layer height selected was of 0.05 mm so as not to allow permeation of water into the device. The models were designed using a mixture of *Onshape* (Present Onshape Inc. 2014) and *Blender* (version 2.8; Blender foundation 2019) and sliced using *Ultimaker Cura* (version 4.3; Ultimaker 2019). The properties of the printer, as well as the slicer settings used are further detailed in Appendix A

Table 1 - Properties of PLA used (Smartfill 2019)

Material	Smartfill Ivory white polylactic acid
Density (g.cm^3)	1.24
Filament Diameter (mm)	2.9
Glass transition temperature (ºC)	55 – 60
Heat distortion temperature (ºC)	55
Break tensile strength (MPa)	53
Young modulus (MPa)	3600
Tensile elongation (%)	6
Print temperature (ºC)	220 $\pm$ 20
Hot pad print temperature (ºC)	0 – 60

The membranes used for the device were the NF-90 (Filmtech 2019) and the FS40PP (Alfa Laval 2019) and are further detailed in Appendix B.

4.1.2 Gluing

Several gluing options were considered for the goal of sealing the device. Several types of sealant were considered, including UV-based adhesives[3], O-rings[4] and silicone[5]. However, according to a previous author (Hams, 2018), a slow-setting 2-part epoxy glue is the most appropriate adhesive for the job, a commonly used glue in the membrane field due to its good wetting characteristics for a plethora of materials (Page, Berg, and Manson 2001). This type of glue proved to have the best mechanical endurance without showing cracks, limiting the leakage inside the device and ideally, such a glue would have limited heat release during the curing time. This holds true for PC-PLA and PLA-membrane connections under standard conditions.

However, for reason explored further into this chapter (section 4.2.2), some gluing required a glue other than the 2-part epoxy, and some of the gluing was done using a cyanoacrylate gel.

In order to select the glues to use, two small rectangular bars (Figure 14) were printed in PLA with dimensions 100.0 x 4.8 x 10.0 mm, creating a contact area of 23.0 mm^2, wielding a pressure of 100.0 bar when lifting a 23 kg weight. The bars were designed in order not to undergo buckling or breaking under the applied localized pressure, cleaned and treated superficially with dichloromethane and then glued together. This test aimed to show which glues resistance to a pressure far superior to the maximum pressure in NF tests (~60 bar).

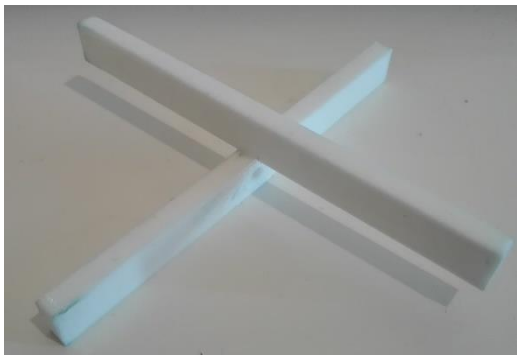

Figure 14 - Bars used for glue pressure test.

Thee glues in total were tested, two epoxy based glues, Araldite Standard (Huntsman Advanced Materials 2011) and Zap Z-Poxy 30 minute formula (Pacer Technology 2019), and a cyanoacrylate based adhesive, Loctite super flex (Henkel 2019). The former due to its pre-selection in a previous study (Hams 2018), where it proved efficient, if slightly flawed due to difficult of application and a sheer strength in plastics between 40 and 60 bar (Huntsman Advanced Materials 2011), which is too close to the average work values (20 - 50 bar). Zap Z-Poxy was selected due to its sheer strength of 170 bar in certain materials, high

[3] UV light cannot permeate PC.
[4] Allowed permeation due to roughness on PLA surface.
[5] Elastic and seals the device properly but develops cracks and preferential paths overtime.

chemical and mechanical resistance and non-shrinking, non-brittle characteristics (Pacer Technology 2019). Lastly, Loctite super flex is a gel based cyanoacrylate which is not only easier to apply in certain situations but proved to have better wetting characteristics in plastics than epoxy based adhesives (Millet 1986). All glues were prepared and cured as stipulated by the manufacturer.

Whereas the Araldite glue failed to fully lift the weight, breaking the connection at around 60% lift, both Zap and Loctite were able to fully lift it momentarily. Ergo, these two glues were selected.

Using these glues, the membranes were glued to the support pieces, cut from the main membrane sheet and the sealed further with a second thin layer of glue on the side boundaries of the support. The membrane area not covered with glue (i.e. effective membrane area A_e) was determined by photographing the membrane and analysing it using *ImageJ* (Rasband 1997) to pixelcount the soiled area.

4.1.3 Device design

The devices used all present with the same basic structure. Following the designs of Completo et al. (2017) and Hams (2018), the devices used are composed of a shell, a lid and a membrane support.

The shell , composed of polycarbonate (Hams 2018), serves to envelop the functional parts of the device. Made from a 50 mL Nalgene round centrifuge tube (Thermo scientific 2001), this tube was fitted with a 1.6 mm hole 23.0 mm from the bottom in order to alleviate pressure during filtration on the permeate side and to easily remove permeate with aid of a syringe.

The lid has a cork-like design, with a lower part that goes into the shell and an upper part that stops the lid from entering further. This top part is ridged to facilitate removal, as it makes it easier to grip. A hole goes through the lid in order to normalise pressure from the retentate side. This hole, 9mm from the centre of the lid, has a conical design with a diameter of 1.5 mm on the top but only 0.4 mm at the bottom. This design, through the action of capillary forces, makes it difficult for fluid to flow through this hole and minimizes leaks from the retentate side. The design can be seen in the figure bellow.

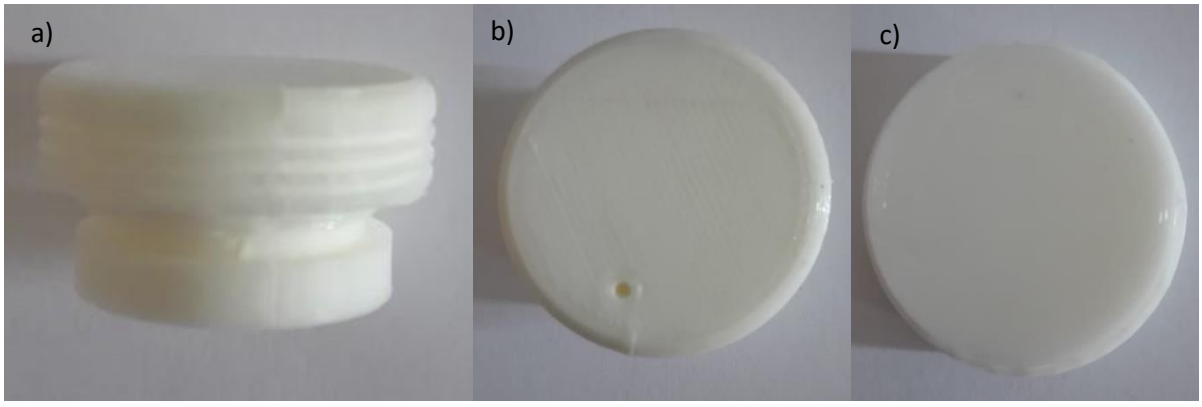

Figure 15 - Lid of prototype UFP – 190823 – A. a) side view; b) top view; c) bottom view;

The membrane support (Figure 16), has the function of keeping the device structurally sound. As such, it needs to be able to sustain any forces. While tensile forces aren't an issue with the current device, the design needed to account for the action of shear and compressive forces.

To combat shear stress, the device was printed fully vertically from the bottom up, utilizing support material to keep it straight throughout. This keeps all layers parallel to the hydrostatic forces and enhances the resistance of the membrane support significantly. The support material was designed specifically for the purpose of being easy to remove whilst maintaining integrity and is detailed in Appendix A.

Compressive forces make up the bulk of the stress felt by the device, and so this part needed to be designed to avoid buckling. This supports were designed at a β angle of 0º. Utilizing the buckling equation (Barkey, Turgeon, and Varun Nare 2008; Yoo and Lee 2011; Zaccaria et al. 2011)

$$F_{max} = \frac{\pi^2 . E . I}{(L . k_c)^2} \qquad (4\text{-}1)$$

where F_{max} is the maximum force the column allows without buckling, E is the Young modulus, I ($=\frac{\pi}{2} . radius^4$ for cylinder) is the second momentum of area, L is the length of the column and k_c (= 0.7 for column restrained on one side) is the effective compression factor, one can calculate the perfect length for this piece to have.

Considering a maximum pressure of 100 bar, a pressure distribution area of around 400 mm^2 and a bottom base with 4.5 mm radius, this translates in about $L \approx 100$ mm. Since this equation does not consider all applied forces and is simply a rough estimation, and in order to roughly maintain the current proportions used by both Completo et al. (2017) and Hams (2018), the actual size was reduced to $^1/_4$ of the maximum allowed size and the support column was designed with a 25 mm support strut. This translates into a maximum allowed permeate volume of 5.2 mL for this design. This conical approach therefore optimizes the previous allowed permeate volume of 2.3 mL (Hams 2018).

Additionally, in order to facilitate gluing further, instead of a net-like support beneath the membrane like used on previous trials, the membrane support for this dissertation was modelled with inbuilt ridges, emulating this net and allowing permeation by stopping the membrane from being compressed against the support surface.

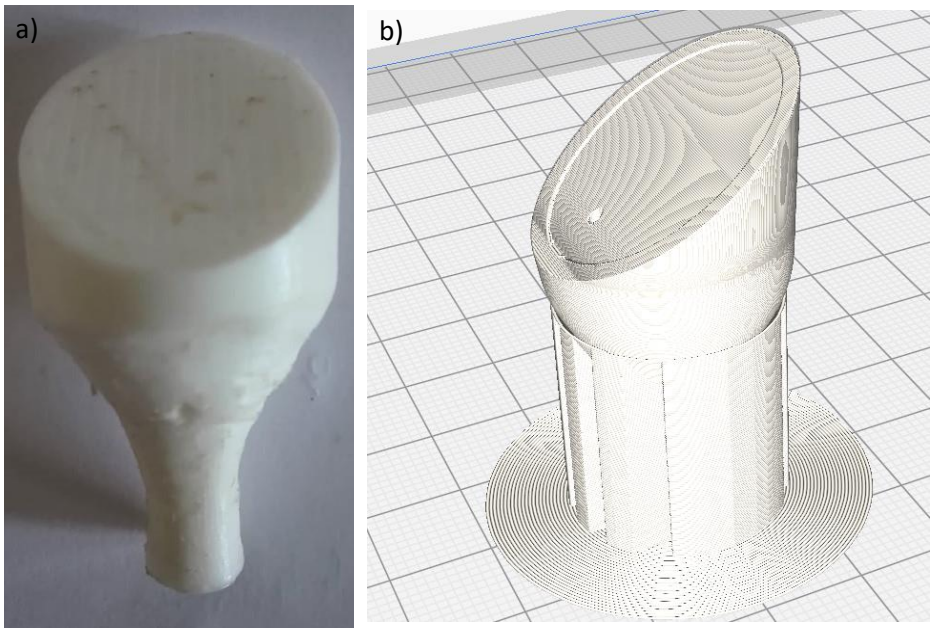

Figure 16 – a) Base support of device UFP – 190823 – A; b) Cura view of supported membrane support of device UFP – 190823 – A.

4.1.3 Experimental Setup

To test the performance of the prototypes, tests were performed at different pressure conditions at 20ºC in a Sorval RC 6 plus Superspeed Centrifuge (Thermo-Scientific 2019a) using a Thermo-Scientific SA-300 fixed angle rotor (Thermo-Scientific 2019b), at a 34º angle (α) (Figure 17). The devices were positioned in such a way that β = 0º, tested one at a time and counterbalanced using a water filled tube, deviating no more than 0.1 g from the device, as specified by the centrifuge specifications (Appendix C) In order to avoid the actions of the Archimedes' screw like lift inside the tube, which could de-stabilize the tube through turbulent forces and cause leaks, the acceleration and deceleration of the centrifuge were set to 3 minutes each. Due to the variations in rotor velocity (limited by the centrifuge), all pressures herein are given the name of nominal pressure and are understood to hold a variation of up to 5%.

Figure 17 - a) RC6 centrifuge (Thermo-Scientific 2019a);
b) SA- 300 rotor (Thermo-Scientific 2019b)

The pressures inside the tube were determined as laid out in section 2.4.1, based on the axial positions of certain points in the tube. r1 varies depending on the height of the liquid meniscus and is calculated geometrically, taking into consideration the angles of said meniscus with respect to the centrifugal force. r2 and r2' are equal to 54.7 mm and 83.0 mm respectfully. When a test is performed at a full chamber (25 mL) with a non-modular system, r1 = 35.6 mm and the graph detailing pressure with respect to centrifuge speed would be:

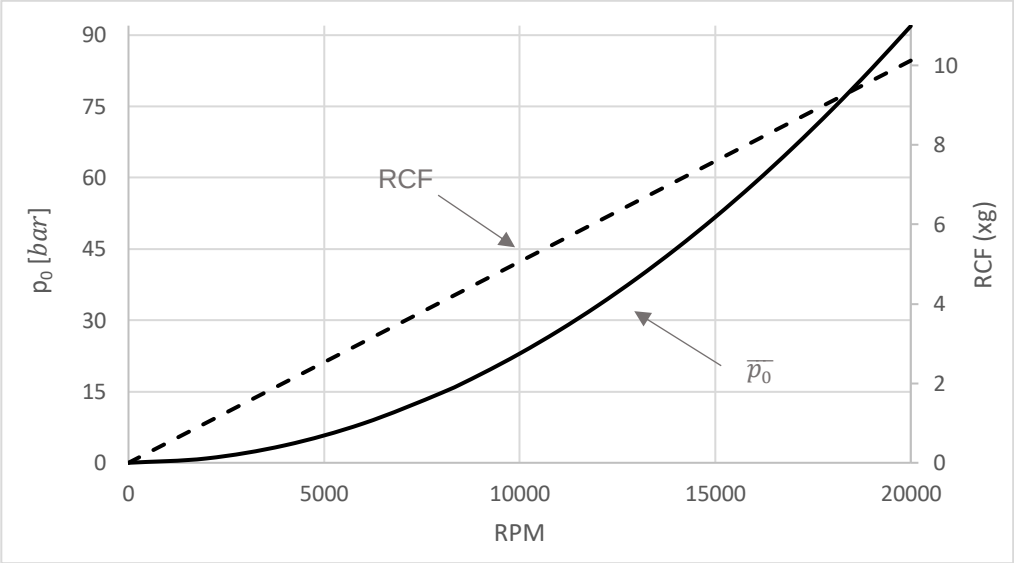

Figure 18 - Graph of pressure and relative centrifugal force relative to centrifuge speed for 25 mL of liquid

It's important to note that, as mentioned before, $\overline{p_0}$ is simply an average measurement of pressure above the membrane and not a definitive measure of pressure. Because of this, it's important to account for higher pressures on certain points of the membrane during tests in order not to damage both the device and the membrane. For instance, in Figure 19 we see an in-depth simulation of the pressure inside the device running at a $\overline{p_0}$ of 40 bar. There, we can note that one edge of the membrane is under 60 bar, which as seen before can lead to irreversible damage through compression or even membrane tearing. Since this point is quite close to the membrane support permeation point, reversible compaction[6] in this location is especially dangerous, as it can reduce the performance of the whole membrane. Therefore, special attention to this fact needs to be taken when dealing with higher pressures in order not to damage the device.

[6] Term compaction is used here to refer to compression of membrane against support, not to membrane compaction as understood in section 2.2.4

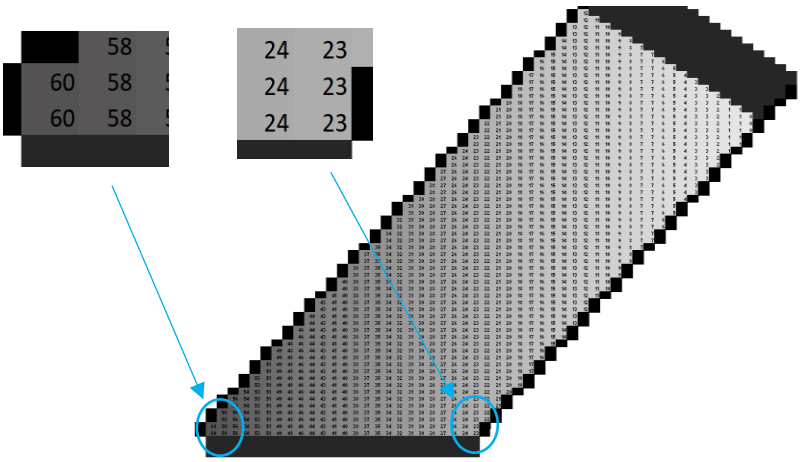

Figure 19 - Simulation of pressure across a fluid-full device running at $\overline{p_0}$ = 40.0 bar, with special attention on the pressure on the edges of the membrane surface. Values are given in bar.

The tests used pure water for both NF and UF and binary aqueous solutions containing Coomassie brilliant blue G-250 (Sigma-Aldrich 2019a) and polyethylene glycol 35k (Sigma-Aldrich 2019b) for NF and UF tests, respectively. The G-250, with a MW of 854 g.mol^{-1}, was prepared by diluting 0.025g of the solute in 100.0 mL of unionized water (conductivity lower than 5 µS.cm^{-1}), in order to wield a negligible osmotic pressure ($\pi_f < 10^{-2}$ bar). The PEG 35k was prepared by diluting 5.360 g in 100.0 mL of unionized water for a 5.0 wt% solution with $\pi_f = 3.7 \times 10^{-2}$ bar.

Unless otherwise stated, the membranes were cleaned using a Ultrasil 110 (Lenntech 2001) dilute solution, carefully scrubbed with a cotton bud and centrifuged with unionized water at 5 bar for 20 minutes.

4.2 Experimental prototype development

4.2.1 Sealed chamber trials

The point of the first performance test was to determine if sealing was possible with a reduced amount of glue. Hams' prototype (Hams 2018) was selected, slightly altered to better suit commercial applications. Firstly, a 2.0 mm ring, 0.6 mm thickness, was fitted above the membrane, which both homogenizes the glue and levels the membrane surface (Figure 20). Secondly, the glue amount was vastly reduced and kept only on the sides of the support, so as not de-stabilize the membrane surface. This model was then fully sealed with epoxy instead of being fitted with a membrane.

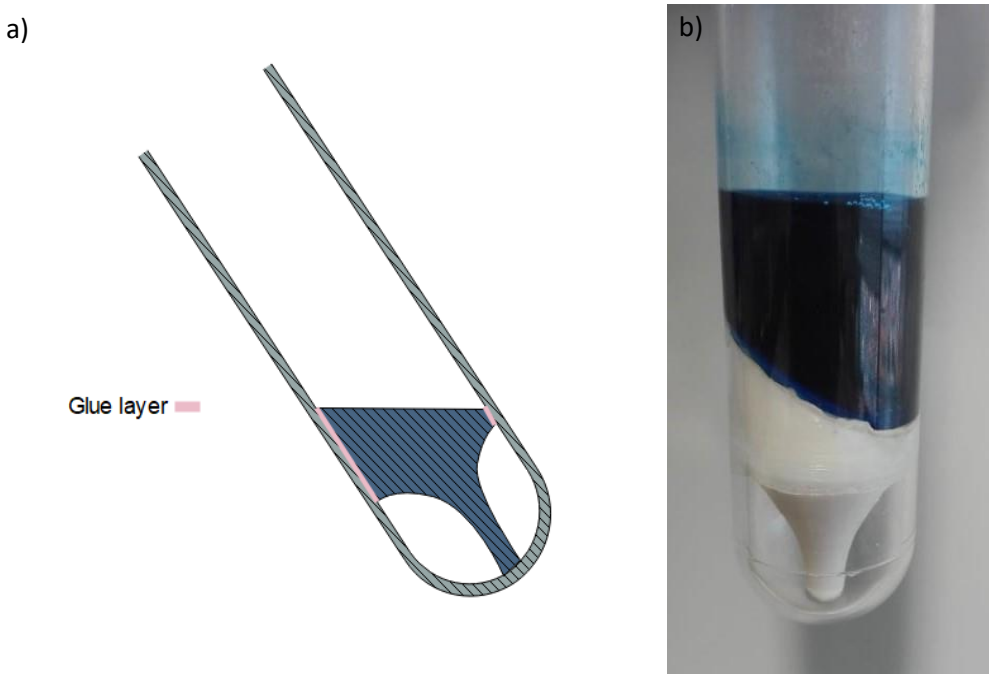

Figure 20 - Visualization of glue layer in a) a diagram showing the device; b) device NFP – 190508 – A – NC filled with a blue G-250 solution pre-trial

The device was tested at different velocities with increments of 1000 rpm starting at 5000 rpm. A G-250 solution was used as a tracer for better visibility and leak detection. The results show that no liquid permeate the device up to 18000 rpm, corresponding to a pressure of 66 bar, showing that the device should remain sealed at working conditions of up to 30 bar.

4.2.2 Open chamber trials

Using the same model as the previous trial, this time fitted with a NF membrane, one wanted to test the pure water permeation of the device. For this purpose, 10 and 20 mL of tracer solution of G-250 were filtered using two similar devices at different pressures at 5 bar intervals. Different filtration times were used to avoid overflowing the chamber. The results are detailed bellow. Since the rejections were evaluated on a purely visual basis, no value is given.

Table 2 – Open chamber result data: Water flux tests in prototypes NFP – 190510 – A and NFP – 190515 – A[7].

	$A_e\ [cm^2]$	$V_f\ [mL]$	$P\ [bar]$	RPM	$t_{run}\ [s]$	$V_p\ [mL]$	$J_s\ [mL.cm^{-2}.h^{-1}]$
NFP – 190510 – A	4.1	10.023	5.0	5210	1200	0.052	0.041
			10.0	7370	1200	0.081	0.062
			15.0	9030	1200	0.153	0.113
			20.0	10400	1200	4.274	3.168
			25.0	11700	600	5.152	7.642
			30.0	12800	120	5.122	37.923
			35.0	13800	60	5.178	76.711
NFP – 190515 – A	3.7	19.963	5.0	4940	3600	0.221	0.060
			10.0	6990	3600	0.392	0.110
			15.0	8260	1200	0.489	0.398
			20.0	9540	1200	4.272	3.447
			25.0	10700	600	5.060	8.181
			30.0	11700	120	4.933	39.883
			35.0	12600	60	5.181	83.938

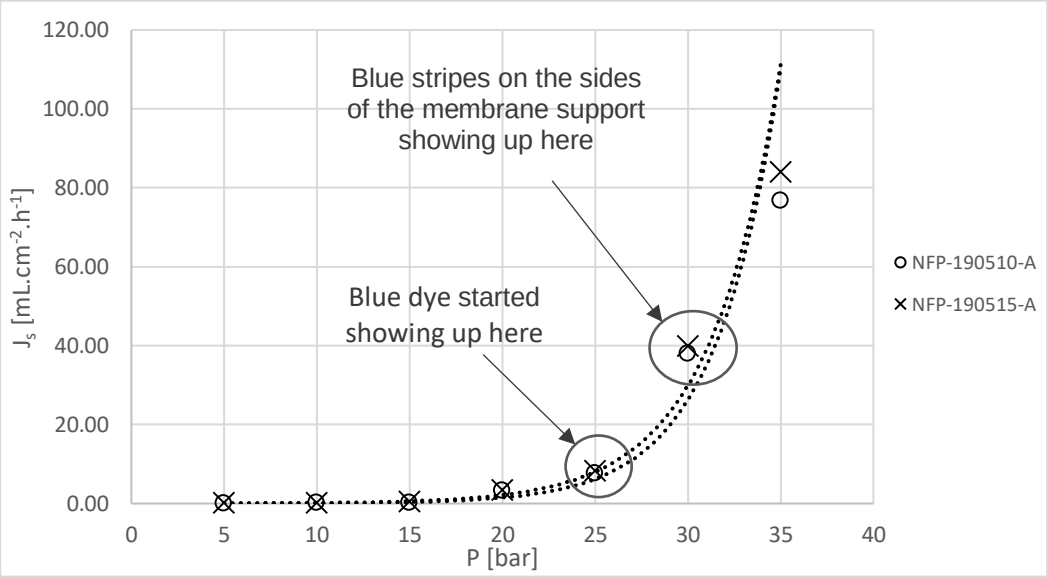

Figure 21 – Open chamber result graph: Water flux tests in prototypes NFP – 190510 – A and NFP – 190515 – A.

Here, we expected to see a linear relationship of Flux with relation to pressure. However, the relationship observed shows an exponential behaviour, starting at around 25 bar, pressure at which blue dye became visible in the permeate. Further tests using the same devices verified that, after the previous tests, flux at 10 bar had highly increased and blue dye permeated. It's therefore safe to assume pressures

[7] No values for uncertainty will be disclosed on data tables unless otherwise stated to avoid needless data cramping. When necessary, these values will be mention on the text. All values in the table are statistically significant

higher than 20 bar damage the gluing of the current device beyond fixability, allowing permeation of the tracer dye through the gaps in the glue.

Further dissection of the membrane concluded that the gluing problem occurred on the membrane-PLA connections for smaller pressure (<30) bar. This was determined by the presence of a blue ring around the membrane on its bottom side, showing that the permeation was through the sides rather than through the membrane. The massive increase in flux from 30 bar onwards is explained by the blue line found from this point on around the membrane support (Figure 22), and shows that the gluing needs to be optimized not just for membrane-PLA connections, but also for the PLA-PC connections, that cannot handle high pressures. This is, presumably, because the PC expands at a different rate than the PLA, causing tension to build up in the glue.

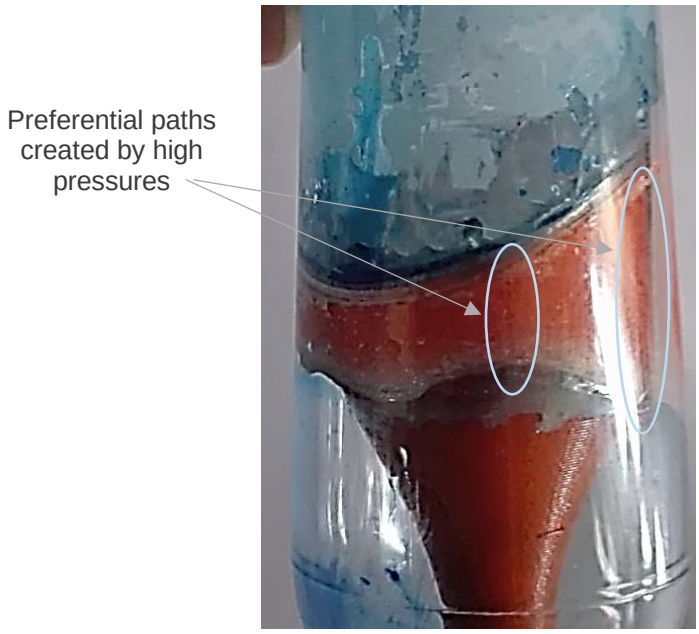

Figure 22 - Some preferential paths formed after exposure to high pressures within the device.

A secondary theory states that as the PLA hydrates, it connects less and less to the epoxy glue, meaning that the more tests performed, the worse the connection becomes. As PLA is somehow permeable to water (Siparsky et al. 1997) it hydrates, despite the printing properties chosen (layer height, printing speed, filling shape and density) minimizing the effect (Gordeev, Galushko, and Ananikov 2018; Stansbury and Idacavage 2016). It appears hydrated PLA affects its connection to epoxy glue and is therefore not as optimal for this particular application as thought before.

Both these effects were considered in further models of the device, and all gluing from section 4.2.3 further was done using cyanoacrylate super glue gel rather than the afore-used epoxy. Likewise, all PC-PLA connections were terminated.

4.2.3 Full-tube model trials

Having considered the complications of the previous model, a new idea arose. This idea was to avoid gluing the PLA pieces to the polycarbonate shell. In order to accomplish this, a PLA tube needed to be designed and fitted inside the shell, connected directly to the membrane support, in order to avoid unnecessary leaks derived from glue problems.

Before any of this could be accomplished, a pre-trial to verify the viability of the design had to be performed. 4 small tubes with an inner diameter of 14.4 mm and height of 50.0 mm were printed with thickness of 0.5, 1.0, 1.5 and 2.0 mm (Figure 23). Then they were filled with water, sealed with Teflon and pressurized by pumping pressurized air into it. Since no water permeated the walls for any of the trial tubes, it's demonstrated that it's possible to run a PLA tube through high pressures without side leaks occurring

Figure 23 – Small 1.0 mm thickness test tube printed to validate glue less test.

Having tested the hypothesis, a new tube was designed (Figure 24). Simply put, it was the same membrane support fitted with a large neck like addon on top. This neck kept the sample inside the PLA tube and created a physical barrier between feed and permeate without any glue. This tube was then fitted with a membrane module (membrane + ring), glued with epoxy and then tested.

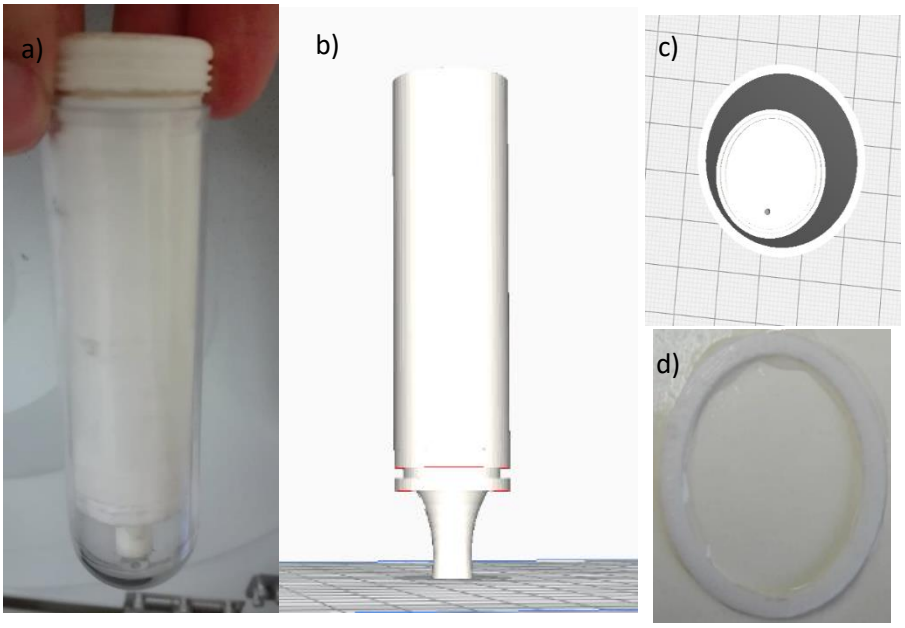

Figure 24 – Several views of the full-tube device a) Side view of printed device; Cura view of the device in b) side view and c) top view; d) Membrane module to be fitted into tube

The reason while no numerical data is presented for this section is because, despite being tested thrice with prototypes NFP – 190626 – A, NFP – 190627 – A and NFP – 190627 – B, the first was fully sealed reproducing tests from section 4.2.1 and showed no permeation and the second and third, despite emulating section 4.2.2, showed equally no permeation. From this, we can conclude that, due to the difficulties involved in gluing the membrane module to the membrane support, even when in a controlled amount, the glue tends to impede membrane flow, making the full-tube model entirely useless.

While this model could be optimized further and could possibly be made to work, a better idea appeared, derived from this one, and far easier to work with and assemble. Therefore, this model served simply as a steppingstone into the modular system explored on section 4.2.4.

4.2.4 Modular system trials

Derived from the previous model, this idea relies on the principle that PLA-PC connections are wildly flawed. Unlike the previous model, however, the support and the sample chamber were fully separated in order to avoid difficult gluing. A further separation of the membrane support was performed, and the single piece became a flat top support and a separate ridged membrane support attached to the sample chamber.

The module piece (Figure 25 – d) consists of a PLA chamber like the one in section 4.2.4 but disconnected from any other parts. This piece contains a 2 mm platform similar to the ring introduced in section 4.2.1.

The flat top support (Figure 25 – c) is virtually an angled cut of the bottom part of the previous membrane support. It retains all the physical integrity of the previous design, without having to be glued to the shell. In turn, the membrane support (Figure 25 – b) corresponds to the part excluded from the top part support, with the added addition of a connection point between itself the module chamber piece. This way, this piece is glued directly to the interior of the module chamber, pressed against the ring and supported by the connecting platform.

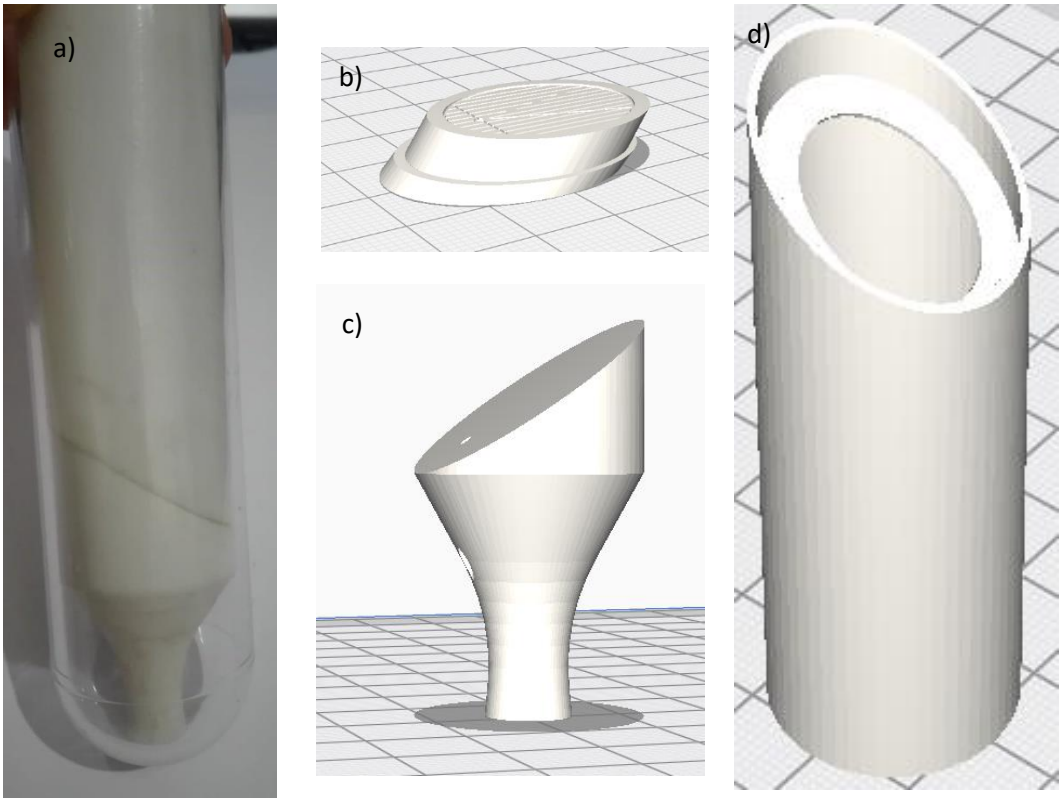

Figure 25 - Several views of the modular device a) Side view of printed device; Cura view of b) membrane support part, c) module support part and d) Module part;

In order to verify the validity of the design, since no other designs of this kind exist yet, UF will be used in order to not use excessive pressures that might muddle the performance, and therefore our judgement of the device. Since it's already demonstrated that the geometry of the device is the key to NF performance (Completo et al. 2017; Hams 2018), this isn't a problem and should only be interesting to study in future approaches. Likewise, these trials aimed only at detecting the flux and the rejection of these prototypes to verify the feasibility of the newer design, hence why pure water flux trials were not done.

The trials were performed on several devices. A 5 wt% PEG35k solution was filtered with a sample volume around 15 mL[8] using said devices under a 5.0 bar pressure for 4 minutes (10 minutes if acceleration

[8] 18 mL for some devices when two devices were tested at once, to allow balance in the centrifuge

and deceleration times are accounted for). Since such a high sample volume was used relative to the maximum allowed permeate volume, no results for CF are presented, as these would be meaningless. CF tests would only be significant when implementing an inner chamber (floating or otherwise), which was not done in the present work.

The results of the modular UF trials are presented bellow in Table 3.

Table 3 – Modular system results data: Centrifuge trials at 5 bar for several UFP prototypes.

	UFP - 190823 – A (1st run)	**UFP - 190823 – A (2nd run)**	**UFP - 190903 - A**	**UFP - 190912 - A**	**UFP - 190912 - B**	**UFP - 190914 - A**
A_e [cm^2]	3.0	3.0	3.2	2.8	2.9	3.0
V_f [mL]	15.163	18.471	15.231	14.978	14.823	17.231
P [bar]	5.0	5.3	5.0	5.0	5.0	5.2
RPM	4990	5030	4990	5030	5030	5030
t_{run} [s]	240	240	240	240	240	240
V_p [mL]	0.243	0.712	0.978	0.789	0.4667	0.7256
i_p [º$brix$]	2.0	1.0	0.6	1.8	1.2	1.1
c_p [$g.L^{-1}$]	2.04	1.01	0.61	1.83	1.22	1.11
J_s [$mL.cm^{-2}.h^{-1}$]	1.206	3.539	4.472	4.252	2.134	3.165
R_a [%]	61.255	80.78	87.95	65.194	75.87	77.90

. The obvious disparity between the 1st run of prototype UFP - 190823 – A and all other runs is the unwashed state of this run. This proves that all membranes need to be washed with the detergent as detailed before, in order to eliminate the protective layer. It also proves that for this small membrane size, under the conditions of these tests, it's not necessary to wash the membrane for the 3h recommended by the manufacturer (Alfa Laval 2019) and a 20 minute cycle will suffice.

Despite having similar conditions, the other results with these tests vary wildly. The flux varies between 2.134$\pm$0.004 mL.cm^{-2}.h^{-1} and 4.472$\pm$0.005 mL.cm^{-2}.h^{-1}. We can easily blame the differences in L_p for this, as due to the small membrane areas being used, there will be sufficient differences in both the number and shape of pores and in the matrix of the membrane to cause significant variation.

As for the rejection, it varies between 65.194$\pm$0.008 % and 87.95$\pm$0.03 %. Even when neglecting the obvious outlier, UFP - 190912 – A, , which we can assume had some sort of large leak based on its high flux and low rejection, the average rejection obtained is still of only of 80.63$\pm$0.02 %. Compared to the expected rejection for solute with the MW of PEG35k of around 100%, these results show that leaks must have occurred in every device. By observing Figure 26, and excluding UFP - 190912 – A, a linear upwards trend becomes visible with relation to J_s. This relationship was predicted by the models explored in section 2.2 and shows, if nothing else, that the bulk of the flow was through the membrane, meaning any leaks must be due to small imperfections in the gluing. This is confirmed by the fact that the fluxes fall within the expected order of magnitude.

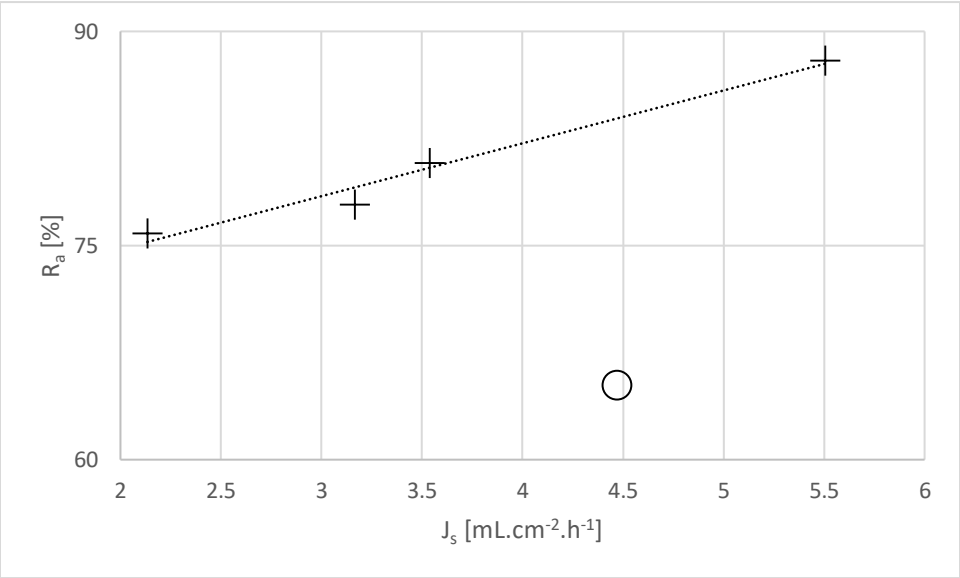

Figure 26 - Apparent rejection plotted against solvent flux of modular approach trials. A linear relationship can be seen in the data. The circle represents the outlier, UFP - 190912 - A

There is a rather large possibility that these small fissures are due to one of three factors: either the gluing area is too small and cannot keep up with the pressures, the pressure baring points are unable to hold the connection or the ridges existent in the PLA print, despite allayed as much as allowed by the printer and slicer settings, created areas not wetted by the cyanoacrylate gel susceptible to permeation.

If it's the former, this ring area must be optimized in relation to the gluing process, in order to create a connection strong enough to resist pressures of up to 30 bar. If it's the latter, then the only possible options are switching the gluing method entirely or substituting the PLA for another material better wetted by the cyanoacrylate gel and with a smoother surface. Both these hypotheses are further discussed in section 4.3.

The problem with pressure baring connection is studied in section 4.2.5.

4.2.5 Final modular approach

As a final approach, a new model was designed in order to aggregate the findings of this dissertation into a working prototype. To this effect, instead of relying on the support to make the binding connection between module and support, relying on the module part leads to the support pressing against the module instead of pressing away from it (Figure 27 – a; Figure 27 – b). This strengthens the connection considerably.

In addition, the ring was also modified. It was designed to surround the support, stopping it from sliding around during the gluing process, this way avoiding potential flaws during the gluing process that might have existed in different trials (Figure 27 – c).

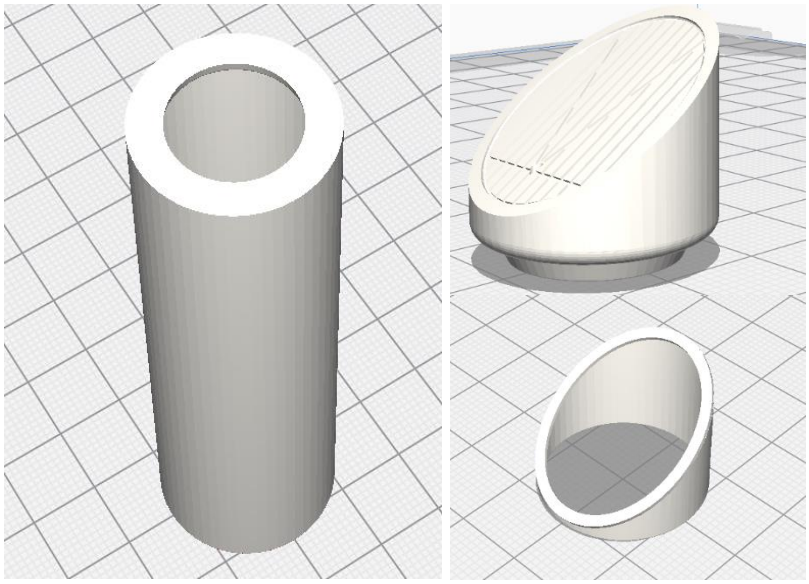

Figure 27 - Cura view of the new modular device a) Module part; b) Membrane support part, c) ring part;

When this device (NFP – 191022 – A) was tested with a nanofiltration membrane at pressure of 20 bar with a blue-250 solution, a similar flux was achieved to that of the average in 4.2.2. The rejection, however, was of nearly 100%, with no discernible micro-leaks visible in the device. Altogether, this means this sealing method is at least capable of resisting the creation of micro-leaks and, allied to everything else, shows that performing centrifugal concentration of small samples is possible using this device.

4.3 Future considerations

Despite showing promising results, there is still much work that must be done on this project in order to make it commercially viable. In this final segment, I propose several improvements on the current model and suggest further testing based on the observations made throughout the development of this project

Firstly, the gluing must be optimized. This involves finding the perfect gluing area for the current cyanoacrylate gel. Tests should be performed for different module ring sizes larger and smaller than the current 2 mm. It should be kept in mind that the larger the ring, the smaller the active membrane area. This indirect relationship between gluing area and membrane area need to be carefully considered when performing these tests. Alternatively, exploration of a different adhesive all together is possible. This adhesive should be able to hold PLA-PLA and PLA-membrane connections up to at least 30 bar without leakage for several sequential tests, even after the PLA becomes hydrated.

Secondly, test pertaining to the inner block should be performed. While empty chamber runs will be able to analyse fluxes and rejections properly enough to analyse if the device works, an inner piece that

extends the height of the sample and minimizes the sample volume will effectively enhance the flux through the membrane (pressure remains higher for longer) and increase the CF vastly.

Moreover, tests to properly ascertain the concentrating capacities of the device should be performed, where CF is calculated for different osmotic pressure and pressure conditions.

After this, optimization of the β angle is mandatory. This angle is responsible for the self-cleaning effect and optimizing this angle will lead to the largest possible flux and rejection in the device. For commercial applications, this translates into a better concentration factor for NF modules and membranes capable of concentrating most, if not all proteins without the addition of non-gelling agents for UF modules. As seen on chapter 3, angles that allow for membranes to be dragged away from the membrane will give better results. In this particular model, these should correspond to $\beta < 0^{o}$.

Other possible test would include, but not limited to: testing several solutes at once; testing fouling resistance; testing protein gelling layer resistance; testing the device for MF, UF and NF; testing different types of internal blocks; testing material resistance to organic solvents.

Finally, a possible material and structure overhaul could be enforced. A more resilient shell could be designed in another material, with a detachable permeate chamber for easy cleaning and permeate recovery. The module itself could be extruded in PC rather than being printed in PLA. This would also optimize the gluing situation previously discussed, as PC is both smother and less hydratable than PLA, making it potentially better for membrane securing. Additionally, other plastics could be explored based on mechanical characteristics and economic viability. Even if it meant losing the fully disposable nature of the device, this proposal would not only massively improve the versatility of centrifugal filtration as a whole, by allowing the same device to be used for any purpose but would also reduce plastic waste in as much as 600% when considering the waste of a disposable device with the waste of a single module.

This page was intentionally left blank

Chapter 5: Conclusion

The main goal of this dissertation started out as being the development of a commercially viable device for batchwise centrifugal nanofiltration. As both the project and the device developed, the goal shifted to developing a commercially viable batchwise centrifugal filtration device capable of performing a range of operations, from large particle and colloid filtration (MF) to concentration of solutes with MW as low as 1000g.mol^{-1} (NF).

Several different models were designed and prepared throughout this work. Apart from the outer PC shells and the membranes, all the pieces needed were printed in PLA and manufactured using a 3D printer and glued using different adhesive types. The devices were subjected to a multitude of tests that led to a final device being submitted as the main result of this thesis.

The device in question is a modular device capable of switching membrane modules in order to perform different types of operations with the same basic material. It is mainly intended to both perform nanofiltration of small samples (< 100 mL) and ultrafiltration of particularly difficult to process solutes, such as proteins which can't be filtered by conventional means because of high gel polarization.

Tested the model at an UF level with filtration runs using a 5 wt% solution of PEG35k showed results with fairly normal fluxes, with an average of 3.59$\pm$0.05 mL.cm^{-2}.h^{-1}. The rejections, however, were a bit low. The expected values were of 100.0%, but the actual rejections averaged at 80.63$\pm$0.02 % and peaked at 87.95$\pm$0.03 %. These low rejections are explained by small fissures in the glue, either due to failure during the gluing process or to the intrinsic irregularity of a printed PLA surface. These fissures were fixed in later runs by restructuring the pressure points of the device and allowing for rejections of nearly 100.0% with NF runs.

The proposed device shows high promise in regard to the objectives laid out on the beginning of this dissertation. Because of the contributions of Completo et al. (2017) and Hams (2018), we know the device's general geometry to be able to highly concentrate low MW solute solutions at a small-volume scale. Due to the membrane position and high pressures and highly negative β angles allowed by this device, non--saline protein treatment should show high mitigation of gel and concentration polarization. Furthermore, by applying the material overhaul discussed in section 4.3, not only can the device become more secure from a mechanical point of view, allowing any current problems to be surpassed, but it would also become less of an environmental and economic burden by reducing plastic consumption in as much as 600%.

All in all, the contraption created for this project shows capable of performing the tasks it aimed to perform and proposes an alternative to the currently used devices by not only performing the same tasks but achieving two entirely new task as yet impossible in most laboratory environments.

The following list summarizes the main conclusions found in this segment:

- A new, innovative prototype capable of performing centrifugal nanofiltration for the concentration of small-samples (<100 mL) and centrifugal ultrafiltration of small-samples of non-saline protein solutions without gel polarization was designed;
- Fluxes were limited only by the membranes used, with mass transport limitations including fouling, concentration polarization and gel-layer polarization being mitigated by the geometry of the device, which is able to achieve rejections of 100%;
- The modular approach facilitates retentate removal, assembly and switching of separation processes, and leads to less plastic waste.

References

Abdelrasoul, A., H. Doan, and A. Lohi. 2013. 'Fouling in Membrane Filtration and Remediation Methods'. In *Mass Transfer - Advances in Sustainable Energy and Environment Oriented Numerical Modeling*, edited by Hironori Nakajima. InTech. https://doi.org/10.5772/52370.

Ahmad, M. 2012. 'Assessment of Mathematical Models for Ultrafiltration of Multi-Solute Continuous Cross-Flow Process'. Canada: University of Waterloo.

Alfa Laval. 2019. 'Flat Sheet Membranes for Ultrafiltration — FS, UFX, RC and ETNA Types'. 23 September 2019. https://www.alfalaval.com/globalassets/documents/products/separation/membranes/flat-sheet-membranes/uf-flat-sheet-membranes_200000311-1-en-gb.pdf.

Ao, L., W. Liu, L. Zhao, and X. Wang. 2016. 'Membrane Fouling in Ultrafiltration of Natural Water after Pretreatment to Different Extents'. *Journal of Environmental Sciences* 43 (May): 234–243. https://doi.org/10.1016/j.jes.2015.09.008.

Baker, R. W. 2004. *Membrane Technology and Applications*. Chichester, UK: John Wiley & Sons, Ltd. https://doi.org/10.1002/0470020393.

Baker, R.W. 2000. 'MEMBRANE SEPARATION'. In *Encyclopedia of Separation Science*, 189–210. Elsevier. https://doi.org/10.1016/B0-12-226770-2/00101-0.

Banerjee, P., and S. De. 2010. 'Coupled Concentration Polarization and Pore Flow Modeling of Nanofiltration of an Industrial Textile Effluent'. *Separation and Purification Technology* 73 (3): 355–362. https://doi.org/10.1016/j.seppur.2010.04.023.

Barkey, M. E., M. C. Turgeon, and T. Varun Nare. 2008. 'Buckling of Stiffened Thin-Walled Truncated Cones Subjected to External Pressure'. *Experimental Mechanics* 48 (3): 281–291. https://doi.org/10.1007/s11340-007-9080-6.

Barr, J., and L. White. 2006. 'Centrifugal Drum Filtration: I. A Compression Rheology Model of Cake Formation'. *AIChE J,* 52: 545–556. https://doi.org/10.1002/aic.10678.

Blender (version 2.8). 2019. Netherlands: Blender Foundation. blender.org.

Bonhomme, L., J. Doyle, K. Greenizen, G. Gagne, S. Devin, G. Lombard, and V. Smith. 2014. Centrifugal Filter. United states patent office US8747670, filed 11 October 2012, and issued 10 June 2014.

Bowers, W., and P. Rigolupos. 1986. Centrifugal microconcentrator and methods for its use. United states patent office US4632761, filed 15 August 1983, and issued 30 December 1986.

Bowers, W., B. Yankoupoulos, and T. Towle. 2001. Ultrafiltration device and method for forming same. United States Patent and Trademark Office US6269957 B1, filed 3 December 1999, and issued 7 August 2001.

Carman, P.C. 1997. 'Fluid Flow through Granular Beds'. *Chemical Engineering Research and Design* 75 (December): S32–S48. https://doi.org/10.1016/S0263-8762(97)80003-2.

Completo, C., V. Geraldes, V. Semião, M. Mateus, and M. Rodrigues. 2017. 'Centrifugal Nanofiltration for Small-Volume Samples'. *Journal of Membrane Science* 540 (October): 411–421. https://doi.org/10.1016/j.memsci.2017.06.069.

Dickhout, J.M., J. Moreno, P.M. Biesheuvel, L. Boels, R.G.H. Lammertink, and W.M. de Vos. 2017. 'Produced Water Treatment by Membranes: A Review from a Colloidal Perspective'. *Journal of Colloid and Interface Science* 487 (February): 523–34. https://doi.org/10.1016/j.jcis.2016.10.013.

Filmtech. 2019. 'FILMTEC™ NF90 Nanofiltration Elements for Commercial Systems'. 23 September 2019. https://www.dupont.com/content/dam/dupont/amer/us/en/products/water-solutions/documents/609-00378.pdf.

Gordeev, E. G., A. S. Galushko, and V. P. Ananikov. 2018. 'Improvement of Quality of 3D Printed Objects by Elimination of Microscopic Structural Defects in Fused Deposition Modeling'. Edited by Michael C. McAlpine. *PLOS ONE* 13 (6): e0198370. https://doi.org/10.1371/journal.pone.0198370.

Hams, S. 2018. 'Development and Optimization of a Centrifugal Nanofiltration Device for Small Volume Samples Master-Thesis'. Lisboa: Technische Universität Dortmund & Instituto Superior Técnico.

Henkel. 2019. 'Technical Data Sheet: Loctite® Power Flex'. 18 September 2019. http://www.farnell.com/datasheets/1675708.pdf.

Hilal, N., O. O. Ogunbiyi, N. J. Miles, and R. Nigmatullin. 2005. 'Methods Employed for Control of Fouling in MF and UF Membranes: A Comprehensive Review'. *Separation Science and Technology* 40 (10): 1957–2005. https://doi.org/10.1081/SS-200068409.

Huntsman Advanced Materials. 2011. 'Araldite Standard - Two Component Epoxy Adhesive'. October 2011. http://www.chemcenters.com/images/suppliers/169257/Araldite%20Standard.pdf.

Kedem, O., and A. Katchalsky. 1961. ‘A Physical Interpretation of the Phenomenological Coefficients of Membrane Permeability’. *The Journal of General Physiology* 45 (1): 143–179. https://doi.org/10.1085/jgp.45.1.143.

Kozinski, A. A., and E. N. Lightfoot. 1972. ‘Protein Ultrafiltration: A General Example of Boundary Layer Filtration’. *AIChE Journal* 18 (5): 1030–1040. https://doi.org/10.1002/aic.690180523.

Lenntech. 2001. ‘P3-Ultrasil-110’. 2001. https://www.lenntech.com/Data-sheets/ECOLAB-P3-ultrasil-110-L-EN.pdf.

Lewis, G. N. 1908. ‘The Osmotic Pressure of Concentrated Solutions, and the Laws of the Perfect Solution’. *Journal of the American Chemical Society* 30 (5): 668–683. https://doi.org/10.1021/ja01947a002.

Lipnizki, F. 2005. ‘Industrial Applications of Ultrafiltration in Pharmaceutical Biotechnology’. *Engineering in Life Sciences* 5 (1): 81–83. https://doi.org/10.1002/elsc.200407047.

Luis, P. 2018. ‘Introduction’. In *Fundamental Modelling of Membrane Systems*, 1–23. Elsevier. https://doi.org/10.1016/B978-0-12-813483-2.00001-0.

Matsuura, T., and S. Sourirajan. 1981. ‘Reverse Osmosis Transport through Capillary Pores under the Influence of Surface Forces’. *Industrial & Engineering Chemistry Process Design and Development* 20 (2): 273–282. https://doi.org/10.1021/i200013a015.

Mehdizadeh, H., and J.M. Dickson. 1989. ‘Theoretical Modification of the Surface Force-Pore Flow Model for Reverse Osmosis Transport’. *Journal of Membrane Science* 42 (1–2): 119–145. https://doi.org/10.1016/S0376-7388(00)82369-8.

Millet, G. H. 1986. ‘Cyanoacrylate Adhesives’. In *Structural Adhesives*, edited by S. R. Hartshorn, 249–307. Boston, MA: Springer US. https://doi.org/10.1007/978-1-4684-7781-8_7.

Murthy, Z.V.P., and S. K. Gupta. 1997. ‘Estimation of Mass Transfer Coefficient Using a Combined Nonlinear Membrane Transport and Film Theory Model’. *Desalination* 109 (1): 39–49. https://doi.org/10.1016/S0011-9164(97)00051-9.

Okada, T., and T. Matsuura. 1991. ‘A New Transport Model for Pervaporation’. *Journal of Membrane Science* 59 (2): 133–149. https://doi.org/10.1016/S0376-7388(00)81179-5.

Pacer Technology. 2019. ‘PRODUCT SALES SHEET: Z-Poxy™ 30Min System’. 17 September 2019. https://www.amcsupplies.com.au/manuals/Z-Poxy%2030%20Min%20System%20-%20TDS.pdf.

Page, S.A., J.C. Berg, and J.A. Manson. 2001. 'Characterization of Epoxy Resin Surface Energetics'. *J. Adhesion Sci. Technol.* 15 (2): 153–170. https://doi.org/10.1163/156856101743382.

Pall Life sciences. 2003. 'Centrifugal Devices for Ultrafiltration & Microfiltration Nanosep®, Microsep™, Macrosep®, and Jumbosep™ Devices'. 2003. http://wolfson.huji.ac.il/purification/PDF/dialysis/PALL_CentrifualDevice.pdf.

Porter, M. C. 1972. 'Concentration Polarization with Membrane Ultrafiltration'. *Industrial & Engineering Chemistry Product Research and Development* 11 (3): 234–248. https://doi.org/10.1021/i360043a002.

Porter, M. C., ed. 1990. *Handbook of Industrial Membrane Technology*. Park Ridge, N.J., U.S.A: Noyes Publications.

Present Onshape Inc. 2014. 'Onshape | Product Development Platform'. 2014. https://www.onshape.com/.

Rasband, W. 1997. *ImageJ*. Wisconsin: Laboratory for Optical and Computational Instrumentation. https://imagej.nih.gov/ij/index.html.

Rigolupos, P. 1970. Self-cleaning Ultrafilter. United states patent office US3488768, filed 8 February 1968, and issued 6 January 1970.

Rudie, B. J., T. A. Torgrimson, and D. D. Spatz. 1985. 'Reverse-Osmosis and Ultrafiltration Membrane Compaction and Fouling Studies Using Ultrafiltration Pretreatment'. In *Reverse Osmosis and Ultrafiltration*, edited by S. Sourirajan and Takeshi Matsuura, 281:403–414. Washington, D.C.: American Chemical Society. https://doi.org/10.1021/bk-1985-0281.ch029.

Sahai, R. 2000. 'MEMBRANE SEPARATIONS | Filtration'. In *Encyclopedia of Separation Science*, 1717–1724. Elsevier. https://doi.org/10.1016/B0-12-226770-2/05151-6.

Scott, K. 1995a. 'INTRODUCTION TO MEMBRANE SEPARATIONS'. In *Handbook of Industrial Membranes*, 3–185. Elsevier. https://doi.org/10.1016/B978-185617233-2/50004-0.

Scott, K. 1995b. 'MEMBRANE MATERIALS, PREPARATION AND CHARACTERISATION'. In *Handbook of Industrial Membranes*, 187–269. Elsevier. https://doi.org/10.1016/B978-185617233-2/50005-2.

Sherwood, T. K., P. L. T. Brian, R. E. Fisher, and L. Dresner. 1965. 'Salt Concentration at Phase Boundaries in Desalination by Reverse Osmosis'. *Industrial & Engineering Chemistry Fundamentals* 4 (2): 113–118. https://doi.org/10.1021/i160014a001.

Sigma-Aldrich. 2019a. ‘Coomassie® Brilliant Blue G 250 (C.I. 42655) CAS 6104-58-1 | 115444’. 2019. http://www.merckmillipore.com/PT/en/product/Coomassie-Brilliant-blue-G-250-C.I.-42655,MDA_CHEM-115444?ReferrerURL=https%3A%2F%2Fwww.google.com%2F.

Sigma-Aldrich. 2019b. ‘Poly(Ethylene Glycol) 35,000 | Sigma-Aldrich’. 2019. https://www.sigmaaldrich.com/catalog/product/aldrich/81310?lang=pt&region=PT.

Siparsky, G., K. Voorhees, J. Dorgan, and K. Schilling. 1997. ‘Water Transport in Polylactic Acid (PLA), PLA/ Polycaprolactone Copolymers, and PLA/Polyethylene Glycol Blends’. *Journal of Environmental Polymer Degradation* 5 (3): 125–136. https://doi.org/10.1007/BF02763656.

Smartfill. 2019. ‘Smartfil PLA’. Accessed 17 September 2019. https://filament2print.com/gb/index.php?controller=attachment&id_attachment=13.

Stansbury, J. W., and M. J. Idacavage. 2016. ‘3D Printing with Polymers: Challenges among Expanding Options and Opportunities’. *Dental Materials* 32 (1): 54–64. https://doi.org/10.1016/j.dental.2015.09.018.

Susanto, H., H. Arafat, E. M. L. Janssen, and M. Ulbricht. 2008. ‘Ultrafiltration of Polysaccharide–Protein Mixtures: Elucidation of Fouling Mechanisms and Fouling Control by Membrane Surface Modification’. *Separation and Purification Technology* 63 (3): 558–565. https://doi.org/10.1016/j.seppur.2008.06.017.

Svarovsky, L. 2001. ‘Centrifugal Filtration’. In *Solid-Liquid Separation*, 432–441. Elsevier. https://doi.org/10.1016/B978-075064568-3/50040-7.

Székely, G., M. Gil, B. Sellergren, W. Heggie, and F. Castelo Ferreira. 2013. ‘Environmental and Economic Analysis for Selection and Engineering Sustainable API Degenotoxification Processes’. *Green Chem.* 15 (1): 210–225. https://doi.org/10.1039/C2GC36239B.

Thermo scientific. 2001. ‘NALGENE Centrifuge Tubes and Bottles’. 2001. catalogus.de/pdf/30/centrifugecatintl.pdf.

Thermo-Scientific. 2019a. ‘Thermo Scientific Sorvall RC6 plus Superspeed Centrifuge’. 2019. https://www.grupo-certilab.com/resources/files/S/CENTRIFUGAS/RC-6%20PLUS.PDF.

Thermo-Scientific. 2019b. ‘SA-300 Fixed Angle Rotor’. 2019. https://www.thermofisher.com/order/catalog/product/18100#/18100.

Tsuru, T., T. Shutou, S. Nakao, and S. Kimura. 1994. 'Peptide and Amino Acid Separation with Nanofiltration Membranes'. *Separation Science and Technology* 29 (8): 971–984. https://doi.org/10.1080/01496399408005611.

Ultimaker Cura (version 4.3). 2019. https://ultimaker.com/software/ultimaker-cura.

Vassarotti, V.. 1997. Centrfugal method for concentrating macromolecules froma solution and dewece for carrying out sad method. United States Patent and Trademark Office US5,647,990, filed 24 May 1994, and issued 15 July 1997.

Volkov, A. 2014. 'Membrane Compaction'. In *Encyclopedia of Membranes*, 1st ed. Berlin: Springer-Verlag.

Wang, J., D. S. Dlamini, A. K. Mishra, M. T. M. Pendergast, M. C.Y. Wong, B. B. Mamba, V. Freger, A.R.D. Verliefde, and E. M.V. Hoek. 2014. 'A Critical Review of Transport through Osmotic Membranes'. *Journal of Membrane Science* 454 (March): 516–537. https://doi.org/10.1016/j.memsci.2013.12.034.

Wijmans, J.G., and R.W. Baker. 1995. 'The Solution-Diffusion Model: A Review'. *Journal of Membrane Science* 107 (1–2): 1–21. https://doi.org/10.1016/0376-7388(95)00102-I.

Yaroshchuk, A. E. 1995. 'Solution-Diffusion-Imperfection Model Revised'. *Journal of Membrane Science* 101 (1–2): 83–87. https://doi.org/10.1016/0376-7388(94)00277-6.

Yoo, C. H., and S. C. Lee. 2011. 'Buckling of Columns'. In *Stability of Structures*, 1–73. Elsevier. https://doi.org/10.1016/B978-0-12-385122-2.10001-6.

Zaccaria, D., D. Bigoni, G. Noselli, and D. Misseroni. 2011. 'Structures Buckling under Tensile Dead Load'. *Proceedings of the Royal Society A: Mathematical, Physical and Engineering Sciences* 467 (2130): 1686–1700. https://doi.org/10.1098/rspa.2010.0505.

Appendices

This page was intentionally left blank

Appendix A – 3D printing parameters

3D printer specifications

Table 4 - Ultimaker 2+ 3d printer specification (Ultimaker 2019)

Model	Ultimaker 2+
Printer dimensions (mm)	342.0 x 493.0 x 588.0
Build volume (mm)	223.0 x 223.0 x 305.0
Weight (kg)	11.3
Print technology	Fused filament fabrication
Optimal filament diameter (mm)	2.9
Layer resolution for .4 mm nozzle (µm)	200 – 20
Layer resolution for .8 mm nozzle (µm)	400 – 20
XYZ resolution (µm)	12.5 x 12.5 x 5.0
Feeder type	Geared
Print head (mm)	Swappable – 0.25, 0.4, 0.6 and 0.8
Maximum build speed ($mm^3.s^{-1}$)	24.0
Nozzle temperature (ºC)	180 – 260
Nozzle heat-up time (min)	< 2
Glass build plate temperature (ºC)	20 – 100
Optimal operating ambient temperature (ºC)	15 – 32
Supported file types	GCODE
Operation Conditions	Standard operating condition for PLA

Slicer specifications

Table 5 - Slicer properties used for modelling 3d printed parts.

Program	Ultimaker Cura
Version	4.3
Nozzle (mm)	0.4
Layer height (mm)	0.05
Infill %	100
Wall thickness (mm)	1.05
Wall line count	3
Top/Bottom thickness (mm)	0.72
Top layers	0
Bottom layers	∞
Horizontal expansion (mm)	0.00
Retraction	Enabled
Print speed (mm/s)	60.0
Z hop when retracted	Disabled
Print cooling	Enabled
Fan speed	100%
Support (when used)	
Placement	Everywhere
Overhang angle	45º
Pattern	Zig zag
Z distance (mm)	0.15
XY distance (mm)	1.00
Support Interface	disabled
Build plate adhesion (when used)	
Type	Brim
Width	Piece width + 5.0 mm

This page was intentionally left blank

Appendix B – Membrane Specifications

Nanofiltration Membrane

Table 6 - Properties of NF membrane used (Alfa-Laval 2019).

Product code	Filmtech NF90-4040
Membrane material	Polyamide
Support material	Polyester
Membrane type	Thin-film composite
Minimum salt rejection (%)	98.7
Flow rate ($m^3.day^{-1}$ for 4.8 bar)	7.6
pH range	2 – 11
Maximum operating temperature (ºC)	45
Maximum operating pressure (bar)	45

Ultrafiltration Membrane

Table 7 - Properties of UF membrane used (Filmtech 2019).

Product code	Alfa Laval FS60PP
Membrane material	Fluoro polymer
Support material	Polypropylene
Membrane type	Porous
MWCO ($g.L^{-1}$)	100k
pH range	1 – 11
Maximum operating temperature (ºC)	65
Typical operating pressure (bar)	1 – 10

This page was intentionally left blank

Appendix C – Centrifuge parameters

Centrifuge specifications[9]

Table 8 – Specifications of RC 6 centrifuge (Thermo-scientific 2019a).

Model	Sorval RC 6 plus Superspeed Centrifuge
Dimensions (mm)	752 x 835 x 1132
Weight (kg)	350
Rotor speed (rpm)	300 – 22000
Minimum speed increments (rpm)	10 (≤ 10000 rpm); 100 (> 10000 rpm)
Speed control accuracy (rpm)	± 25
Maximum RCF (xg)	55200
Maximum capacity (mL)	4 x 1000
Temperature range (ºC)	-20 – +40
Minimum temperature increments (ºC)	1
Temperature control accuracy (ºC)	± 2
Optimal operating ambient temperature (ºC)	15 – 40
Rotors	Adaptable
Weight difference between opposing rotors (g)	0.1

Rotor specifications

Table 9 - Specifications of SA-300 rotor (Thermo-Scientific 2019b).

Model	Thermo-Scientific SA-300 fixed angle rotor
Material	Aluminium
Weight (kg)	5.5
Bucket dimensions (mm)	29 x 108
Capacity	6 x 50 mL
Minimum radius (mm)	23.5
Maximum radius (mm)	96.7
Maximum speed (rpm)	25000
Maximum RCF (xg)	67509
K factor	573
Angle	34º
Maximum weight allowence	6 x 115 g

[9] These control options were not subjected to any verification or calibration while in use for the purposes of this thesis.

This page was intentionally left blank

Appendix D – Solute data

Coomassie Brilliant Blue R-250

Table 10 - Properties of coomassie brilliant blue G-250 (Sigma-Aldrich 2019a).

MW (g.mol^{-1})	854
Bulk density (g.L^{-1})	520
Solubility (g.L^{-1})	40

PEG 35k

Table 11 - Properties of PEG 35k (Sigma-Aldrich 2019b).

MW (g.mol^{-1})	35000
Bulk density (g.L^{-1})	500
Density (g.cm^{-3})	1.2
Solubility (g.L^{-1})	500

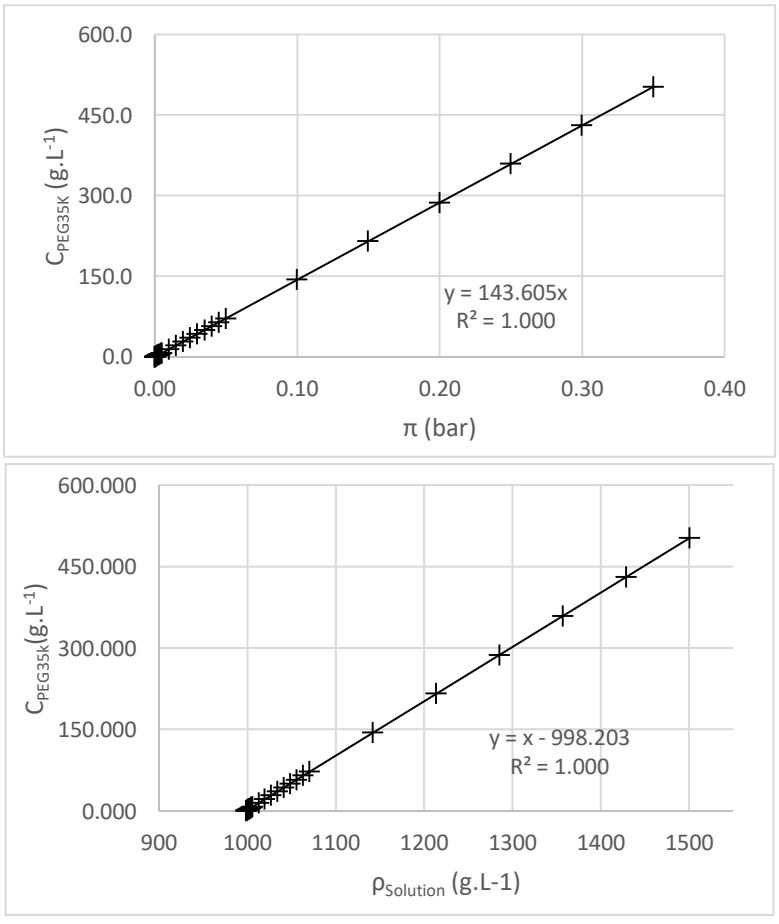

Figure 28 - Osmotic pressure and density of different PEG 35k solutions

This page was intentionally left blank

Appendix E– Calibration curves

PEG 35k

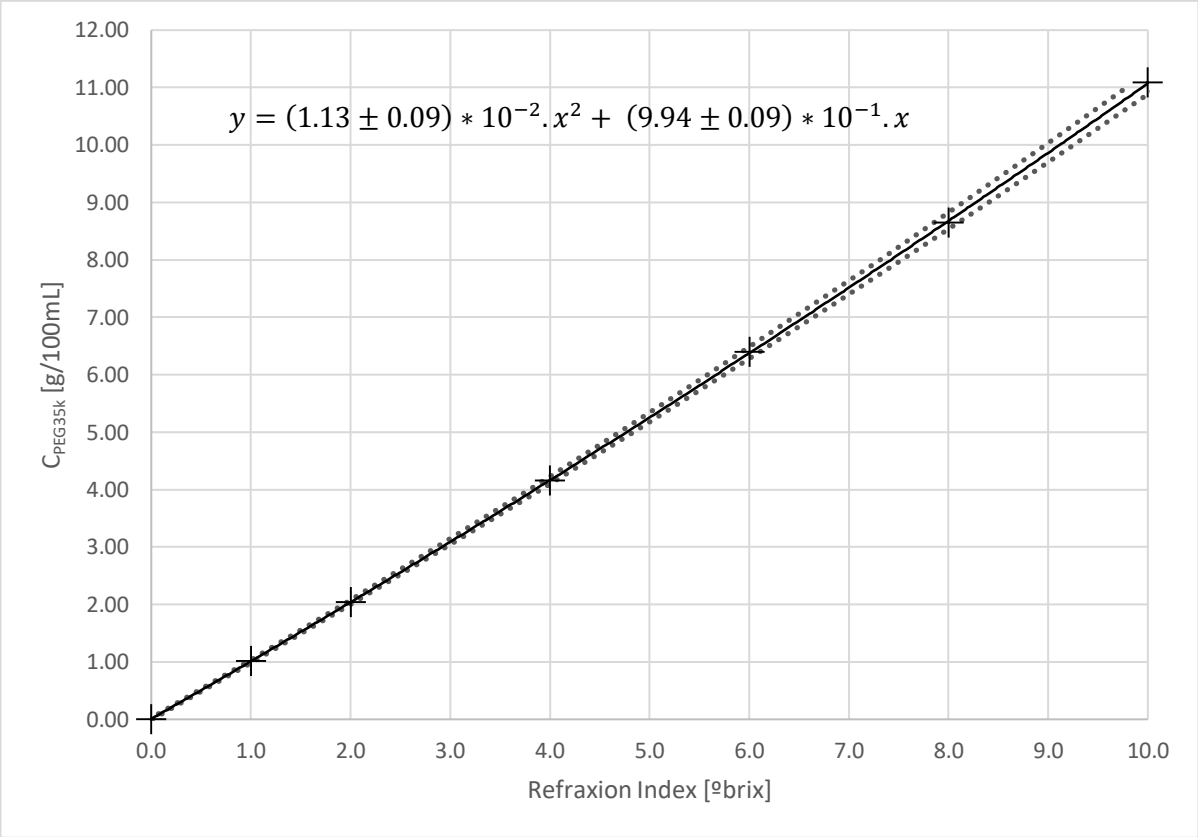

Figure 29 - Calibration of refractometer measurements for PEG 35k.

This page was intentionally left blank

Appendix F – Uncertainty propagation

All lab results obtained in this dissertation were certified using uncertainty propagation. The uncertainty for each result, even if omitted (as is the case in tables) was calculated based on the following factors:

- All samples were prepared by weighing the solute and measuring the volume of the solvent, and then diluting one into the other. The weighing was done with an uncertainty of $\sigma_{scales} = 0.0001\ g$ and the volumes were measured with uncertainty $\sigma_{pipete} = \sigma_{volumetric\ balloon} = 0.1\ mL$.
- All feeds, permeates and retentates were weighed with $\sigma_{scales} = 0.0001\ g$ and the volumes were calculated based on solute density (Appendix D). The permeates were collected with a 1mL syringe with $\sigma_{syringe} = 0.01\ mL$;
- Refractometer measurements were obtained with $\sigma_{refractometer} = 0.1\ °Brix$;
- The pressure was calculated using a trapezoid method to 1000 points, so any uncertainty associated with this calculation dissipates.

This page was intentionally left blank

Appendix G – Prototype Codes

The prototypes were coded in order to easily distinguish between them. They have a filtration type identifier and a date identifier and a lot identifier. This way, the first UF device produced on 5/6/2019 would be labelled UFP – 190605 – A, where UFP stands for ultrafiltration prototype. Likewise, the second NF device produced on the 17/8/2019 would be labelled NFP – 190817 – B. This convention was held anytime a specific prototype is mentioned.

This page was intentionally left blank

Appendix H – Prototype sizes detailed

Table 12 - Dimensions of parts printed throughout this work. Sizes are detailed as sliced. Printed sizes have a variation of 0.02 mm as specified by printer specifications in appendix A.

Shell		**Outer diameter [mm]**	28.70
		Inner diameter, top [mm]	25.60
		Inner diameter, bottom [mm]	25.00
		Spherical bottom height [mm]	1.50
		Height [mm]	85.00
Lid		**Top diameter [mm]**	28.70
		Bottom diameter [mm]	variable
		Ridge size [mm]	0.80
		Ridge deph [mm]	0.80
		Ridge number	3
		Unridged top height [mm]	3.00
4.2.1 **4.2.2**	**Lid**	**Bottom diameter [mm]**	25.5
	Membrane support	**Top diameter [mm]**	25.13
		Bottom diameter [mm]	9.00
		Eliptical a diameter [mm]	30.31
		Eliptical b diameter [mm]	25.12
		Hole position from centre [mm]	8.16
		Hole position from centre (elipse) [mm]	7.56
		Hole radius [mm]	1.20
	Ring	**Height [mm]**	0.60
		a diameter [mm]	30.00
		b diameter [mm]	24.66
		Thickness [mm]	2.00
4.2.3	**Lid**	**Bottom diameter [mm]**	25.4
	Membrane support / inner tube hybrid	**Membrane support**	Same as 4.2.1 / 4.2.2, adjusted for the 1.00 mm edge when needed
		Inner tube height [mm]	75.00
		Inner tube inner diameter [mm]	23.129
	Ring / Membrane module	**Height [mm]**	0.60
		a diameter [mm]	27.75
		b diameter [mm]	21.98
		Thickness [mm]	2.00
4.2.4	**Lid**	Same as 4.2.3	
	Membrane support base	Same as 4.2.1 / 4.2.2, sliced at 34º on circular base, bottom	
	Membrane support disc	Same as 4.2.1 / 4.2.2, sliced at 34º on circular base, top	
	Module	Same as 4.2.3,unconnected to support, ledged ring	
4.2.5	**Lid**	Same as 4.2.4	
	Membrane support base	Same as 4.2.4	
	Membrane support disc	Same as 4.2.4, adjusted 1.0 mm less, curved at the bottom	
	Ring	Fitted around membrane support disc. 1.0 mm thickness	
	Module	Same as 4.2.4, curved and ledged at the bottom	

This page was intentionally left blank